JPET Fast Forward. Published on August 28, 2012 as DOI: 10.1124/jpet.112.197590

JPET#197590

Title Page

The autophagy-senescence connection in chemotherapy; must tumor cells (self) eat before they sleep?

Rachel W. Goehe, Xu Di, Khushboo Sharma, Molly L. Bristol, Scott C. Henderson, Kristoffer Valerie, Francis Rodier, Albert R. Davalos and David A. Gewirtz

Department of Pharmacology and Toxicology
Virginia Commonwealth University (RWG, KS, DAG)

Department of Radiation Oncology
Virginia Commonwealth University (KV, RWG)

Center of Drug Evaluation and Research
Food and Drug Administration (XD)

Department of Pathology
Virginia Commonwealth University (MLB)

Department of Anatomy and Neurobiology
Virginia Commonwealth University (SCD)

Département de Radiologie
Université de Montréal (FR)

CRCHUM et Institut du cancer de Montréal (FR)

Lawrence Berkeley National Laboratory
Berkeley Laboratories (ARD) (ARD)

Running Title Page

Running Title: Adriamycin induced senescence and autophagy

To whom correspondence should be addressed at:
Dr. David Gewirtz
Virginia Commonwealth University
Massey Cancer Center
401 College St.
Richmond, VA 23298

Phone: 804-828-9523
Fax: 804-827-1134
Email: gewirtz@vcu.edu

Number of Text pages: 34

Number of Tables: 0

Number of Figures: 8 with 5 Supplemental

Number of References: 62

Number of words in Abstract: 188

Number of words in Introduction: 475

Number of words in Discussion: 1339

JPET Fast Forward. Published on August 27, 2012 as DOI: 10.1124/jpet.112.197590
This article has not been copyedited and formatted. The final version may differ from this version.

Abstract

Exposure of MCF-7 breast tumor cells or HCT-116 colon carcinoma cells to clinically relevant concentrations of Adriamycin or Camptothecin results in both autophagy and senescence. In order to determine whether autophagy is required for chemotherapy-induced senescence, reactive oxygen generation induced by Adriamycin was suppressed by N-acetyl cysteine and glutathione, and the induction of ATM, p53 and p21 was modulated pharmacologically and/or genetically. In all cases, autophagy and senescence were collaterally suppressed. The close association between autophagy and senescence indicated by these experiments appears to reflect their collateral regulation via common signaling pathways. The potential relationship between autophagy and senescence was further interrogated through pharmacologic inhibition of autophagy with chloroquine and 3-MA and genetic ablation of the autophagy-related genes ATG-5 and ATG-7. However, inhibition of autophagy by pharmacological and genetic approaches could not entirely abrogate the senescence response, which was only reduced and/or delayed. Taken together, our findings suggest that autophagy and senescence tend to occur in parallel, and furthermore that autophagy appears to accelerate the development of the senescent phenotype; however, these responses are not inexorably linked or interdependent, as senescence can occur even when autophagy is abrogated.

JPET Fast Forward. Published on August 27, 2012 as DOI: 10.1124/jpet.112.197590
This article has not been copyedited and formatted. The final version may differ from this version.

Introduction

Cellular senescence is defined as a biological state in which cells have lost the ability to divide, but remain metabolically active for a prolonged period of time (Evan and d'Adda di Fagagna, 2009). Three general types of senescence have been identified, replicative senescence, oncogene-induced senescence and premature (accelerated or stress-induced) senescence (Gewirtz et al., 2008). Replicative senescence describes a proliferative arrest that is due to telomere shortening after a genetically pre-determined number of cell divisions in non-transformed cells (Shay and Roninson, 2004). Oncogene-induced senescence reflects the capacity of the cells to undergo senescence in the presence of the expression of oncogenes such as Ras, ostensibly in an effort to delay transformation (Lee et al., 1999). Premature, accelerated or stress-induced senescence occurs through exposure of the cells to exogenous cytotoxic agents generally associated with DNA damage (Gewirtz et al., 2008; Campisi and d'Adda di Fagagna, 2007).

Autophagy is a catabolic process involving the degradation of a cell's own components through the lysosomal machinery (Glick et al., 2010). Autophagy can be either a cytoprotective or cytotoxic response to chemotherapy or radiation (Gewirtz et al, 2009). While apoptosis and autophagy are highly regulated processes that may crosstalk to determine the ultimate cell fate (Thorburn, 2008), a relatively limited number of reports in the literature have suggested the potential existence of a direct relationship between autophagy and senescence. Specifically, an increase of autophagic vacuoles and senescence-associated beta-galactosidase activity was observed in aging fibroblasts (Gerland et al., 2008). Markers of autophagy and senescence were collaterally observed in bile duct cells of patients with primary biliary cirrhosis as well as in biliary epithelial cells isolated from mice and treated with either hydrogen peroxide or etoposide (Sasaki et al., 2010). Gosselin et al. reported the generation of autophagic vesicles in dying senescent keratinocytes (Gosselin et al., 2009), and Patschan et al. have observed autophagy markers in senescent endothelial cells (Patschan et al, 2008). In addition, Lu et al. reported that the Ras homolog, ARHI, promoted autophagic cell death in ovarian cancer cells in culture and contributed to tumor dormancy *in vivo*, although there were no direct assessments of senescence (Lu et al., 2008).

Of perhaps the most direct relevance to the current work, Young et al. reported the up regulation of autophagy related genes during oncogene-induced senescence and that inhibition of autophagy delayed the senescence phenotype (Young et al., 2009). Since autophagy is often considered to be a cytoprotective response to stress while stress-induced senescence could also reflect efforts by the cell to evade direct cell killing (Gewirtz, 2009; Kroemer and Levine, 2008), the current studies utilizing both breast tumor and colon cancer cells were designed to determine the potential relationship between the autophagy and senescence responses of tumor cells exposed to the anti-tumor drugs, Adriamycin and Camptothecin. More specifically, this work addressed the question of whether senescence was dependent on autophagy.

JPET Fast Forward. Published on August 27, 2012 as DOI: 10.1124/jpet.112.197590
This article has not been copyedited and formatted. The final version may differ from this version.

Methods

Cell culture and treatment MCF-7 cells were purchased from ATCC and cultured in RPMI 1640 supplemented with 5% (v/v) FBS (Gemini Bio-Products, 612112), 5% (v/v) BCS (Lonza, 14-401F), 100U/mL penicillin G sodium and 100ug/mL streptomycin sulfate (Invitrogen, 15140). HCT-116 cells were purchased from ATCC and cultured in RPMI-1640 supplemented with 10% FBS and L-glutamine (0.292mg/ml), 100U/mL penicillin G sodium (Invitrogen), and 100ug/mL streptomycin sulfate (Invitrogen). All cells were maintained at less than 80% confluency at 37°C under a humidified 5% CO2 atmosphere. Twenty-four hours after plating, cells were exposed to 1μM ADR or 5μM Camptothecin for 2 hours, rinsed twice with PBS and maintained in complete medium for the indicated time points. In certain experiments, ADR treatment was preceded with 5μM chloroquine (Sigma Aldrich, C6628-50G), 5mM 3-MA (Sigma Aldrich, M9281), 20μM KU-55933 (Calbiochem, 118500), or 4mM caffeine (Sigma Aldrich, C-0750).

Western Immunoblotting After the indicated treatments, cells were washed with phosphate buffered saline (PBS) and lysed with mammalian protein extraction reagent (M-PER) (Thermo Scientific) containing protease and phosphatase inhibitors. Protein concentrations were determined by the Bradford Assay (Bio-rad). Total protein lysates (10μg) were then diluted in SDS sample buffer and dry boiled for 10 minutes. Protein samples were subjected to SDS-PAGE, transferred to polyvinylidene difluoride membrane (PVDF), and blocked in 5% milk/1xPBS/0.1% Tween (M-PBS-T) for 1 hour. The membrane was incubated with: anti-p62 (1:1000, SCBT, sc-28359), anti-p21 (1:1000, BD-Biosciences, 610234), anti-pRB (1:1000, BD Pharmingen, 554136), anti-p53 (1:1000, BD Pharmingen, 554293), anti-Beclin-1 (1:1000, BD Biosciences, 612112) anti-β-actin (1:1000; Sigma Aldrich). The membrane was then incubated with a secondary antibody of horseradish peroxidase-conjugated goat anti-rabbit IgG antibody (1:5000; Sigma Aldrich) or goat anti-mouse (1:5000; Sigma Aldrich) for 1 hour, followed by extensive washing with PBS-T. Immunoblots were developed using Pierce enhanced chemiluminescence reagents and Bio-Max film.

Detection and quantification of acidic vesicular organelles by staining with Acridine Orange For quantification of AVOs, treated cells were trypsinized, harvested, and washing with PBS at approximately $1x10^6$ cells/mL. Pellets were resuspended in PBS and staining with final

JPET Fast Forward. Published on August 27, 2012 as DOI: 10.1124/jpet.112.197590
This article has not been copyedited and formatted. The final version may differ from this version.

concentration of 1:10,000 acridine orange (Sigma, 01663). Samples were incubated for 15 minutes before analyzed by flow cytometry. Flow cytometry was performed by BD FACS Canto II using BD FACS Diva software at the VCU Flow Cytometry Core Facility. A minimum of 10,000 cells within the gated region were analyzed. For detection of AVOs using fluorescent microscopy, treated cells were stained with acridine orange at a final dilution of 1:10,000 and allowed to incubate at 37ºC for 15 min. After extensive washing with PBS, cells were examined and imaged under a fluorescence microscope (Olympus). All images within a given figure were taken at the same magnification.

Transmission Electron Microscopy (TEM) TEM services including sample fixation, embedding, ultramicrotomy and staining were provided by the VCU Department of Anatomy and Neurobiology Microscopy Facility. Sections were imaged using Joel JEM-1230 TEM equipped with a Gatan UltraScan4000SP 4 K X 4 K CCD camera. The magnification of each image is indicated by the scale bar at the bottom of the micrograph.

Detection and quantification of senescent cells For detection of senescence associated β-galactosidase (SA-β-gal) positive cells, treated cells were washed with PBS and fixed with 2% formaldehyde/0.2% glutaraldehyde/PBS for 5 min. Cells were washed and stained with 5-bromo-4-chloro-3-inolyl-b-$_D$-galactoside (X-gal) in demethylformamide (20mg/mL), 40mM citric acid/sodium phosphate, pH 6.0, 5mM potassium ferrocyanide, 5mM potassium ferricyanide, 150m M NaCl, 2mM $MgCl_2$ and incubated at 37ºC for 24 h. After incubation, cells were washed with PBS and imaged using an Olympus inverted microscope. All images within a given figure were taken at the same magnification. For quantification of SA-β-gal, cells were treated as described above and analyzed using fluorescent β-galactosidase activity marker C_{12}FDG. The protocol was adapted from Debacq-Chainiaux et al.,(2009). Briefly, plated cells were pretreated with 100nM bafilomycin A1 for 1 h in culture medium at 37□C, 5% CO2 followed by treatment with C_{12}FDG at a final concentration of 10μM for 1 h. Cells were washed with 1XPBS and harvested by trypsinization followed by centrifugation. Cells were resuspended in PBS at a concentration of 1 X 10^6 cells/mL and analyzed on BD FACS CantoII. Cells populations were gated on a two parameter display of forward scatter versus side scatter. From the gated population, at least 10,000 cell events were depicted on a histogram where the y-axis

JPET Fast Forward. Published on August 27, 2012 as DOI: 10.1124/jpet.112.197590
This article has not been copyedited and formatted. The final version may differ from this version.

indicates cell count and the x-axis indicated C_{12}-fluorescin fluorescence intensity. β-galactosidase activity was estimated using the mean fluorescent intensity of the population.

RFP-LC3 Redistribution The MCF-7 cell line stably expressing RFP-LC3 was a generous gift from Dr. Keith Miskimins. Cells were treated as described above, fixed in 3% paraformaldehyde, and visualized using an Olympus inverted fluorescent microscope.

Monodansylcadaverine Staining for the detection of acidic vesicular organelles Treated cells were incubated with complete medium containing 1μg/mL monodansylcadaverine (MDC) for 15 min at 37ºC. After incubation, cells were washed with PBS, fresh medium was added, and fluorescent micrographs were taken using an Olympus inverted fluorescence microscope. All images within a given figure were taken at the same magnification.

DCF Staining for Detection of Reactive Oxygen Species Intracellular ROS production was determined by flow cytometry using DCF-DA as the fluorescent probe. Cells (1×10^6) were treated appropriately and incubated with the probe for 30 min at 37□C. Subsequently, cells were washed and resuspended in PBS and analyzed for mean fluorescence intensity using BD FACS Canto II at the VCU Flow Cytometry Core Facility. The median fluorescence intensity was quantified by FACS Diva software of the recorded histograms.

Immunofluorescence Microscopy Cells were seeded on chambered slides (Lab-Tek, 154526), fixed with 3% paraformaldehyde for 10 min, and permeabilized with 0.1% Triton X-100 for 5 min. Slides were blocked with 1% BSA/PBS for 1 hour at RT, and incubated overnight at 4 □C with the following primary antibodies: mouse monoclonal γ-H2AX (1:1000, Millipore, 05-636) and mouse monoclonal 53BP1 (1:100, Novus Biologicals, NB100-904). After extensive washing with PBS, secondary antibodies labeled with Alexa 488 (1:500, Invitrogen, A11001 or Alexa 555 (1:500, Invitrogen, A21428) were added, and slides were incubated for 1 h at RT. Slides were mounted with mounting media and images were acquired at RT with an Olympus inverted fluorescence microscope.

Statistical Analysis Statistical differences were determined using StatView statistical software. The data were expressed as the means ± SD (as standard deviation of the mean). Comparisons were made using a one-way ANOVA followed by Tukey-Kramer post hoc test. P-values ≤ 0.05 were taken as statistically significant.

JPET Fast Forward. Published on August 27, 2012 as DOI: 10.1124/jpet.112.197590
This article has not been copyedited and formatted. The final version may differ from this version.

Results

Autophagy and senescence are collaterally induced in MCF-7 breast cancer cells by Adriamycin. Previous studies from our laboratory as well as others have established the capacity of Adriamycin (ADR) to promote premature or accelerated senescence in tumor cells (Gewirtz, 2009; Chang et al., 1999; Elmore et al., 2002; Di et al., 2009) while a number of studies have indicated that ADR also promotes autophagy (Di et al., 2009; Qian and Yang, 2009). We have postulated that both autophagy and senescence may represent efforts by the tumor cell to evade drug or radiation-induced toxicity (Gewirtz, 2009) and it is well-established that different modes of cell death may coexist in the same cancer cell population in response to genotoxic stress (Di et al, 2009; Jinno-Oue et al., 2010). Furthermore, a number of studies have suggested that autophagy and senescence could be closely related events in aging cells as well as in response to various modes of stress (Garland et al., 2003; Gosselin et al., 2009; Young et al., 2009). Consequently, we assessed whether senescence and autophagy were coincident responses in MCF-7 breast cancer cells when exposed to pharmacological concentrations of the topoisomerase II poison, Adriamycin.

Figures 1A – D indicate that ADR induces both senescent and autophagic responses in a time-dependent manner. Specifically, **Figure 1A** indicates a time-dependent increase in β-galactosidase staining and senescence-associated cell morphology alterations. **Figure 1B, Left and Right Panels,** demonstrates that ADR significantly increased the population of senescent cells over a period of 72 hours (from 2.8% to 61.4%) based on FACS analysis. ADR treatment also induced acidic vesicular organelle formation in MCF-7 cells as assayed by acridine orange staining (AOS) (**Figure 1C**). AOS quantification by FACS analysis demonstrated that ADR increased autophagic vesicle content (from 2.4% to 53.2%) over the 72 hour period subsequent to drug exposure in close parallel with the promotion of senescence (**Figure 1D, Left and Right Panels**). Consistent with these observations, ADR triggered the formation of autophagosomes/autolysosomes as visualized by RFP-LC3 punctate formation in MCF-7 cells that stably express the fusion protein as well as by electron microscopy (**Figure 1E**). These initial observations suggested that autophagy and senescence might be collaterally induced responses upon exposure to Adriamycin.

JPET Fast Forward. Published on August 27, 2012 as DOI: 10.1124/jpet.112.197590
This article has not been copyedited and formatted. The final version may differ from this version.

As an increase in autophagic vesicles formation can indicate either promotion of autophagy or interference with vesicle degradation, autophagic flux was assessed based on degradation of p62 (Mizushima et al., 2010). p62 (SQSTM1) is an oligomerizing signaling adaptor protein that binds to ubiquitin and LC3-II (Panvik et al., 2007). One important function of p62 in regards to autophagy is its ability to shuttle ubiquinated proteins to the proteasome and autophagosomes (Seibenhener et al., 2004); hence, its status is an indicator of autophagic flux. As shown in **Figure 1F**, immunoblotting analyses revealed the degradation of p62 to be maximal between 48 and 72 hours post ADR treatment. In addition, we examined the capacity of ADR to induce p21 and to promote dephosphorylation of Rb, two well-accepted biochemical markers of senescence (Kuilman et al., 2010). p21 interferes with cell cycle progression by inhibiting cyclin dependent kinases (CDK) while the dephosphorylation of Rb occurs when the CDKs are inhibited (Roninson, 2002). **Figure 1F** demonstrates a time-dependent increase in p21 and a decline in pRB levels when MCF-7 cells are exposed by ADR. These results indicate that both autophagy and senescence are collaterally induced by ADR in MCF-7 breast cancer cells.

Suppression of free radical generation interferes with ADR-induced senescence and autophagy. Our laboratory has previously reported that ADR-induced senescence is associated with the generation of reactive oxygen species (ROS) (Di et al., 2009). To further investigate the potential autophagy-senescence relationship, we assessed the impact of the free-radical scavengers, GSH or NAC, on ADR-induced senescence and autophagy. As shown in **Supplemental Figure 1A**, a time-dependent increase of ROS was observed in MCF-7 cells exposed to ADR, based on the intensity of 2', 7'-dichlorofluorescin (DCF) fluorescence followed by FACS analysis. A peak level of ROS was evident at 96h post ADR treatment. Repression of ROS generation by GSH or NAC prior to ADR exposure was observed by fluorescent microscopy (**Supplemental Figure 1B**).

Although there are no clear-cut direct pharmacologic inhibitors of senescence, our laboratory has previously shown that NAC and GSH suppressed ADR-induced senescence in MCF-7 cells (Di et al., 2009). Moreover, NAC has also been reported to attenuate cellular senescence induced in fibroblasts by the alkylating agent, busulfan (Probin et al., 2007). Thus, we hypothesized that GSH or NAC could be utilized to probe the putative association between ADR-induced senescence and autophagy. **Figure 2A, Left Panel** shows that both GSH and

JPET Fast Forward. Published on August 27, 2012 as DOI: 10.1124/jpet.112.197590
This article has not been copyedited and formatted. The final version may differ from this version.

NAC significantly blocked ADR-induced senescence as assayed by β-galactosidase staining. Specifically, both NAC and GSH inhibited ADR-induced senescence by between 50-60% over the course of 5 days (**Figure 2A, Right Panel**) as quantified by C_{12}FDG-fluorescin fluorescence. These results were also reproduced in HCT-116 colon cancer cells (**Supplemental Figure 1C**). Consistent with the effect on the senescence response to ADR, GSH and NAC blocked ADR-induced upregulation of p53, p21, and downregulation of pRb, all of which are associated with stress-induced senescence in MCF-7 cells (**Figure 2B**).

To further address the putative relationship between chemotherapy-induced autophagy and senescence, the effects of GSH and NAC on ADR-induced autophagy were evaluated by acridine orange staining utilizing fluorescence microscopy and FACS analysis. A marked reduction in AOS formation in MCF-7 cells (**Figure 2C)** by GSH and NAC was reproduced in HCT-116 colon cancer cells (**Supplemental Figure 1D**). Time-course studies by FACS analysis revealed that addition of NAC or GSH significantly decreased AVO formation induced by ADR (by 49.5% and 56.08% respectively) over the course of 5 days (**Figure 2C, Lower Panel**).

In additional studies, the autophagic flux (reduction in p62 levels) induced by ADR was partially inhibited by pretreatment with either GSH or NAC (**Figure 2D**). To further confirm the collateral inhibition of ADR-induced autophagy and senescence by free radical scavengers, we utilized MCF-7 cells stably transfected with RFP-LC3. **Figure 2E** demonstrates that pretreatment with GSH or NAC prior to ADR effectively abrogated ADR-induced autophagy based on the pronounced reduction of autophagic puncta formation in the cytoplasm. Taking these findings together, we observe collateral modulation of ADR-induced autophagy and senescence when ROS generation is inhibited.

Influence of the DNA damaging signaling pathway on ADR-induced autophagy and senescence. Adriamycin is a topoisomerase II inhibitor that induces DNA double strand breaks, with consequent activation of the DNA damage signaling pathway (Kurz et al., 2004). ATM, one of the early sensors of DNA damage, has been implicated in the regulation of both autophagy (Alexander et al., 2010) and senescence (Crescenzi et al., 2008). Specifically, it has been reported that ATM knockout prevents the induction of autophagy in response to ROS (Alexander et al.,2010). With regards to senescence, silencing of ATM caused senescent tumor cells to re-enter the cell cycle (Crescenzi et al., 2010).

JPET Fast Forward. Published on August 27, 2012 as DOI: 10.1124/jpet.112.197590
This article has not been copyedited and formatted. The final version may differ from this version.

A number of downstream target substrates are phosphorylated by ATM, including histone γ-H2AX, 53BP1, and p53 (Banin et al., 1998; Burma et al., 2001; Lee et al., 2009). To further interrogate the potential relationship between autophagy and senescence in response to ADR, we first confirmed that ADR induces ATM and its downstream effectors in MCF-7 cells. **Supplemental Figure 2A** demonstrates foci formation for p-ATM, γ-H2AX and 53BP1 in response to ADR in MCF-7 cells, which confirms activation of the DNA damage signaling pathway. To determine whether suppression of ATM might collaterally suppress autophagy and senescence in response to ADR, caffeine and KU-55933 were utilized to inhibit ATM activity. Caffeine is a well-established inhibitor of the activity of both ATM and ATR kinases (Wang et al., 2008) while KU-55933 is a highly specific ATM inhibitor (Hickens et al., 2004). **Supplemental Figure 2B** demonstrates a marked reduction in p-ATM foci when MCF-7 cells were treated with either KU-55933 or caffeine in combination with ADR, confirming that these agents are indeed suppressing the functions of ATM. **Figure 3A, Upper Panel** demonstrates the capacity of both caffeine and KU-55933 to inhibit ADR-induced senescence, as indicated by the decreased β-galactosidase staining, and effects on the cell size and flattened phenotype of the senescent cells. Quantification of the extent of inhibition of senescence induction by Adriamycin by both KU-55933 and caffeine is presented in the **Lower Panel** of **Figure 3A**. While ADR produced a significant increase in senescent cells, the senescent cell population was decreased from 78% to 31% and 20%, respectively in cells that were also treated with either KU-55933 or caffeine. Furthermore, the induction of both p21 and p53 by ADR was also attenuated with the combination treatments as seen in **Figure 3B**. These results are in agreement with the studies by Crescenzi et al. (2008) and the recent findings by Zhan et al. (2010), which link ATM activation to senescence.

To examine whether senescence and autophagy are altered in parallel after ATM inhibition, we again employed acridine orange staining. **Figure 3C** demonstrates that both caffeine and KU-55933 significantly inhibit ADR-induced autophagy as demonstrated by acridine orange staining. Quantification of AVO formation by FACS analysis (**Figure 3D**) confirmed these findings. MCF-7 cells treated with ADR demonstrated a significant increase in red fluorescence, whereas when exposure to ADR was preceded by treatment with either KU-55933 or caffeine, the intensity of red fluorescence was reduced from 50.95% to 7.28% and 18.32%, respectively (**Figure 3D, Left and Right panels**). In addition, as shown in **Figure 3E**,

JPET Fast Forward. Published on August 27, 2012 as DOI: 10.1124/jpet.112.197590
This article has not been copyedited and formatted. The final version may differ from this version.

the reduction in p62 levels induced by ADR was antagonized by both caffeine and KU-55933, consistent with the premise that interference with the DNA damage pathway can collaterally suppress both autophagy and senescence. These results further establish that both autophagy and senescence are downstream responses mediated via the DNA damage signaling pathway.

To further confirm the association between the DNA damage signaling pathway and both senescence and autophagy, shRNA was utilized to downregulate ATM in MCF-7 cells. In contrast to shRNA scramble cells, depletion of ATM caused a significant decrease in senescence as assayed by β-galactosidase staining (**Figure 3F**) and correspondingly blocked autophagy in response to ADR as quantified by FACS analysis of acridine orange stained cells (**Figure 3G**). Thus, the fact that suppression of senescence by ATM depletion collaterally blocked autophagy and senescence further supports the premise that the two may be linked pathways.

Attenuation of Adriamycin-induced autophagy by p21 shRNA. Induction of p21 is a well-established response to ADR (Ravizza et al., 2004). Previous studies from our laboratory showed a robust accumulation of p21 post ADR treatment in association with senescence in both p53 wild type MCF-7 cells as well as in breast tumor cells lacking functional p53 (Elmore et al., 2002). Downstream of ATM, the induction of p21 is generally considered to be a critical component of the senescence response pathway (Macip et al., 2002). Furthermore, up-regulation of p21 has been reported to result in ROS accumulation and a senescence response in both normal and tumor cells (Macip et al, 2002). In order to determine susceptibility to autophagy in cells lacking p21, a MCF-7 cell line stably expressing p21 (shp21) was generated. p21 expression was markedly reduced (by approximately 70%) in the shp21 cells (**Figure 4A**) and, as expected, ADR failed to induce p21 (**Figure 4A**). As would be expected in cells where p21 induction is attenuated, the extent of senescence induced by ADR was markedly reduced in the shp21 cells (**Figure 4B, Left and Right Panels**). Quantification by FACS analysis indicated a greater than 50% reduction of senescence cells in MCF-7 shp21 cells in comparison to senescence in the shControl cells (**Figure 4B, Right Panel**). Furthermore, the morphology of the ADR treated shp21 MCF-7 cells appeared to be different from that of the wild-type MCF-7 cells in terms of reduced flattening and extensions and the absence of cell enlargement (**Figure 4B, Left Panel**). These findings, indicating that a blockade to p21 induction suppresses senescence, were confirmed in HCT-116 cells as shown in **Supplemental Figure 3A**.

JPET Fast Forward. Published on August 27, 2012 as DOI: 10.1124/jpet.112.197590
This article has not been copyedited and formatted. The final version may differ from this version.

With regards to autophagy, shp21 MCF-7 cells demonstrated a significant decrease in autophagy as indicated by the reduced acridine orange staining shown in **Figure 4C (Upper Panel)**. In addition, FACS analysis demonstrated approximately a 50% decrease in the extent of autophagy in the shp21 MCF-7 cells in comparison to shControl cells (**Figure 4C, Lower Panel**). Similar results were generated in the p21-/- HCT-116 colon cancer cells (**Supplemental Figure 3B**).

In addition to p21, p53 is a central element in promoting the senescent phenotype (Gewirtz et al., 2008). Our previous studies have demonstrated that either breast cancer cells where p53 is inactivated by the E6 protein or in which p53 is mutated, ADR-induced senescence was essentially abrogated in the bulk of the tumor population in favor of apoptotic cell death (Elmore et al., 2002). Furthermore, as demonstrated above, induction of p21 downstream of p53 is a fundamental requirement for ADR to induce senescence. We therefore evaluated whether interference with senescence by knockdown of p53 affects ADR-induced autophagy. **Supplemental Figure 3C, Upper Panel** confirms that, as would be expected, silencing of p53 significantly blocked senescence in response to ADR in MCF-7/E6 cells. Moreover, MCF-7/E6 cells demonstrated a dramatically attenuated ADR-induced autophagy (**Supplemental Figure 3C, Lower Panel**). These observations were confirmed by experiments in the p53 knockout or p21 knockout HCT-116 colon cancer cells (**Supplemental Figure 3A and 3B**), where collateral attenuation of ADR-induced senescence and autophagy was evident.

Influence of autophagic inhibitors on Adriamycin-induced senescence. The studies presented to this point suggested the existence of a close relationship between autophagy and senescence; this appears to be likely due to the association of autophagy and senescence with common signaling pathways that involve reactive oxygen generation, ATM phosphorylation and the induction of p53, and p21. To further interrogate the possible linkage between autophagy and senescence, we evaluated whether suppression of autophagy using both pharmacological and genetic inhibition would interfere with ADR-induced senescence. **Figure 5A** demonstrates the impact of inhibition of autophagy by 3-methyl-adenine (3-MA), a PI3K/Akt inhibitor or chloroquine (CQ), a late-stage autophagic inhibitor that blocks the fusion of autophagosomes and lysosomes (Carew et al., 2010; Petiot et al., 2000). The addition of either CQ or 3-MA reduced the extent of AVO accumulation in the cytoplasm of MCF-7 cells exposed to ADR (**Figure 5A**).

JPET Fast Forward. Published on August 27, 2012 as DOI: 10.1124/jpet.112.197590
This article has not been copyedited and formatted. The final version may differ from this version.

Figure 5A (**Lower Panel**) presents FACS analysis indicating that ADR treatment increased the intensity of red fluorescence from 5.1% to 52% while the addition of either 3-MA or CQ decreased the intensity of red fluorescence to approximately 9% and 16% in ADR treated cells, respectively. Lastly, we assessed the combination effects of 3-MA and CQ with ADR on p62 expression levels. ADR treatment alone significantly reduced p62 levels (**Figure 5B**), as in **Figure 3E**. However, both 3-MA and chloroquine attenuated the capacity of ADR to promote autophagy flux (suppression of p62). These experimental strategies resulted in transient effects on senescence, with attenuation of β-galactosidase staining at day three, *but where the extent of senescence was essentially equivalent to that in the cells exposed to ADR alone by day 5* (**Figure 5C**). Immunoblotting analyses showed that both 3-MA and CQ treatment produced a reduction in p53 and p21 levels 72h post ADR treatment (**Figure 5D**), which could account, in part, for the delayed senescence response.

Additionally, as inhibition of drug or radiation-induced autophagy often has been shown to sensitize tumor cells through the promotion of apoptosis (Amarvardi et al., 2007; Xi et al., 2011), we examined the impact of these experimental strategies on apoptosis, in order to eliminate the trivial explanation that the basis for the collateral suppression of autophagy and senescence was that the cells were simply dying. However, minimal apoptosis or cell death occurred with ADR treatment in combination with the autophagy inhibitors CQ or 3-MA (data not shown).

Silencing of ATG5 or ATG7 delayed but failed to block senescence. The studies presented in **Figure 5** suggest that interfering with autophagy may delay senescence but that *senescence can occur independently of autophagy*. Because of the likelihood of off-target effects of the pharmacological inhibitor, we next silenced the essential autophagic protein ATG5 in MCF-7 cells utilizing shRNA. Stable downregulation of shATG5 in MCF-7 cells resulted in an approximately 70% knockdown of ATG5; furthermore, ADR treatment was incapable of inducing ATG5 (**Figure 6A**). As would be expected, a significant reduction of punctuated acridine orange staining was observed in ATG5 knockdown cells exposed to ADR (**Figure 6B**). This was accompanied by decreased senescence staining in MCF-7 shATG5 cells on Day 3 and Day 5 post ADR treatment (**Figure 6C**). Quantification of senescence by FACS analysis in **Figure 6C, Lower Panel** confirmed the visual observations presented in **Figure 6C, Upper**

JPET Fast Forward. Published on August 27, 2012 as DOI: 10.1124/jpet.112.197590
This article has not been copyedited and formatted. The final version may differ from this version.

Panel. However, as with pharmacological inhibition of autophagy, *senescence was delayed but not abrogated* (comparing the extent of senescence at Day 5 in the shATG5 cells with that on day 3 in the shControl cells) despite the fact that autophagy remained essentially suppressed **(**comparing **Figure 6C, Lower Panel** with **Figure 6B, lower panel).**

To further corroborate the above results, we utilized the MCF-7 shATG7 cells as an alternative knockdown model (**Figure 7A**). **Figure 7B (Upper Panel)** shows a significant reduction of orange red puncta formation in the cytoplasm of ATG7 silenced cells, which was confirmed by FACS analysis (**Figure 7B, Lower Panel**). **Figure 7C** confirms that silencing of ATG7 interfered with the capacity of ADR to induce depletion of p62. However, as with the studies using ATG5 knockdown cells, inhibition of ATG7 activity *delayed but did not abrogate* ADR-induced senescence (**Figure 7D, Upper and Lower Panels**). That is, by Day 5, the extent of senescence in the shATG7 cells was similar to that in the shControl cells at day 3 (**Figure 7D, Upper Panel**) and FACS analysis (**Figure 7D, Lower Panel**).

Suppression of autophagy delayed senescence in CPT treated MCF-7 cells. To further confirm the conclusion that suppression of autophagy only delays but does not abrogate senescence, we utilized the DNA topoisomerase I poison, Camptothecin (CPT). Both the promotion of senescence based on β-galactosidase staining and FACS analysis (**Figures 8A and 8B,** left and right panels) and the induction of autophagy (**Figure 8C and 8D,** left and right panels) increased in parallel in a time-dependent fashion. Treatment of MCF-7/shATG5 cells with CPT did not significantly induce autophagy (**Figure 8E,** upper and lower panels) but only delayed senescence (**Figure 8F*, upper and lower panels***), where senescence at day 5 was only slightly below that observed in the corresponding shControl cells. These results indicate that while autophagy can contribute to the establishment of senescence, autophagy is not an absolute requirement since the senescence response is only delayed. The data in **Figure 8G** confirm that silencing of ATG5 interferes with the capacity of Camptothecin to promote autophagic flux based on p62 degradation (comparing the shATG5 and shControl cells).

The delay but not abrogation of senescence in MCF-7 cells in which autophagy was suppressed was confirmed in additional studies utilizing Camptothecin with pharmacological inhibitors in MCF-7 cells. **Supplemental Figure 4A** shows that Camptothecin induced an autophagic response characterized by increased red punctuate staining in MCF-7 RFP-LC3 cells.

A delayed senescence response was observed when autophagy induced by Camptothecin was blocked by CQ or Bafilomycin A1 (**Supplemental Figure 4B**).

JPET Fast Forward. Published on August 27, 2012 as DOI: 10.1124/jpet.112.197590
This article has not been copyedited and formatted. The final version may differ from this version.

Discussion

Our laboratory as well as others have demonstrated that treatment of tumor cells with Adriamycin preferentially induces senescence rather than apoptotic cell death (Chang et al., 1999; Elmore et al., 2002; Su et al., 2009). In addition, previous studies in thyroid cancer and hepatoma cells have demonstrated that Adriamycin can induce autophagy (Qian and Yang, 2009; Lin et al., 2009). Although senescence and autophagy are generally considered to be two distinct cellular events in response to genotoxic stress, there has been accumulating evidence that the two are functionally intertwined (Gerland et al., 2003; Gosselin et al., 2009; Patschan et al., 2008; Jinno-Oue at al., 2010). Specifically, Young et al. reported that autophagy was considered an effector mechanism of senescence and contributed to the establishment of oncogene-induced senescence in both cultured cells and *in vivo* (Young et al., 2009) Moreover, Sasaki et al. demonstrated that autophagy mediates the process of cellular senescence characterizing bile duct damages in primary biliary cirrhosis (Sasaki et al., 2010). Our studies were designed to determine whether autophagy and senescence were collaterally influenced and interdependent responses to chemotherapy.

One incentive for examining the premise of a linkage between autophagy and senescence was our recent findings linking Adriamycin induced senescence with reactive oxygen generation (Di et al., 2009). Our studies found that both GSH and NAC markedly suppressed the senescence response to Adriamycin in both p53 wild type and p53 deficient cells (Di et al., 2009). These observations are consistent with studies in the literature indicating that a rise in ROS level accelerates the onset of the senescence phenotype (Lu et al., 2008; Kurz et al., 2004); that is, ROS may function as messenger molecules activating specific redox-dependent targets that induce senescence (Colavitti and Finkel, 2005). Our current work demonstrates that Adriamycin induced a time-dependent increase of ROS, which is highly consistent with previous similar findings (Song et al., 2005). Furthermore, the antioxidants NAC and GSH prevented ADR-induced upregulation of p53, p21 and downregulation of Rb, all of which are associated with senescence. However, we cannot fully rule out the possibility that these agents provide protection against additional modes of drug action. Kurz et al. demonstrated that NAC could attenuate ADR-induced phosphorylation and activation of γ-H2AX, Chk1 and Chk2 in breast cancer cells, all of which were mediators of DNA damage response pathway (Kurz et al., 2004),

suggesting actions of this compound that were perhaps not directly related to suppression of ROS generation.

With regard to autophagy, it has recently been shown that autophagy is often mediated by ROS and that many stresses that induce ROS generation also induce autophagy (Azad et al., 2009; Karna et al., 2010). Camptothecin has also been reported to significantly induce ROS generation in MCF-7 cells (Akbas et al., 2005; Somasundaram et al., 2002). More recently, Luo et al. found that autophagy regulates ROS-induced cellular senescence via p21 in a p38 MAPKα dependent manner (Luo et al., 2010). Specifically, Luo et al. studies demonstrated that ATG5 siRNA inhibited not only autophagy but also senescence induced by H_2O_2 primarily by blocking the up-regulation of the expression of p21. In the current work, the antioxidants GSH and NAC significantly inhibited ADR-induced senescence and autophagy. In addition, we found that GSH and NAC suppressed the Adriamycin-induced increase in p53 and p21. These observations suggest that ROS may play a central role in mediating both ADR-induced senescence and autophagy responses. However, ROS could collaterally influence both senescence and autophagy through the DNA damage response pathway, and therefore these experiments do not prove that senescence and autophagy are necessarily linked pathways.

It has been suggested that senescence is essentially a DNA damage response (d'Adda di Fagagna 2008), which would be consistent with data implicating ATM, p53, p21 and Rb in mediating senescence (Gewirtz et al., 2008). As an upstream regulator of p53 and primary mediator of the DNA damage response pathway, ATM has been closely associated with the senescence response (Crescenzi et al., 2008; Zhan et al., 2010; Mallette et al., 2007). Silencing of ATM effectively resulted in evasion of senescence in response to constitutive *activation of certain* mitogenic genes in human fibroblasts (Mallette et al., 2007). Abolition of ATM or other DNA damage pathway related genes abrogated oncogene-induced senescence in normal fibroblast (DiMicco et al., 2006). A similar study by Zhan et al. showed that blocking ATM activity prevented hydrogen peroxide induced senescence in vascular endothelial cells (Zhan et al., 2010). Here, we show that pharmacological inhibitors of ATM or shATM efficiently inhibit ADR-induced senescence.

Studies have also suggested a possible linkage between ATM and autophagy. For example, Bandhakavi et al. found that the inhibition of mTOR (which otherwise blocks autophagy) also leads to the upregulation of ATM phosphorylation and substrates (Bandhakavi et

JPET Fast Forward. Published on August 27, 2012 as DOI: 10.1124/jpet.112.197590
This article has not been copyedited and formatted. The final version may differ from this version.

al. 2010). Here, we found that inhibition of ATM by means of pharmacological inhibitors or shRNA reduced ADR- and CPT-induced autophagy. These results confirm a critical role of ATM as a mediator of both senescence and autophagy in response to DNA damaging agents.

The collateral effects of blocking ATM and ROS generation on senescence and autophagy may simply indicate that ROS and ATM signal to both pathways in the cells. Since the induction of cellular senescence and autophagy in MCF-7 by CPT and ADR was associated with an increased expression of p53 and p21, we investigated the senescent and autophagic responses to Adriamycin in cells where p53 or p21 function had been attenuated. Our findings demonstrate that p53 null cells treated with Adriamycin have a significant reduction in both the senescence and autophagic responses. Similarly, in MCF-7 cells exhibiting reduced p21 levels, both ADR-induced autophagy and ADR-induced senescence are significantly attenuated. Again, although these studies suggest the existence of a close relationship between autophagy and senescence, these data may simply reflect the possibility of similar signaling pathways (reactive oxygen induction, ATM, p53 and p21) influencing both pathways independently. A schematic cartoon depicting the regulatory pathway induced by either Adriamycin or Camptothecin leading to senescence, as elucidated by our work, is shown in **Supplemental Figure 5**.

To more rigorously assess the potential requirement of autophagy for senescence, we utilized ATG5 and ATG7 shRNA stable cell lines. ATG5 and ATG7 autophagic related genes have been demonstrated to be essential for the autophagic process (Komatsu et al., 2005; Kuma et al., 2002). We found that ADR treated shATG5 and shATG7 cells showed a substantial delay in the promotion of senescence in comparison to shControl cells, but that a blockade to autophagy does not abrogate the capacity of the cells to senescence. Nevertheless, these data do suggest that autophagy contributes to the establishment of senescence arrest and are in agreement with a recent report from Narita and colleagues (Young et al., 2009). These investigators reported that attenuating autophagy in ER:Ras IMR90 cells by shRNA against ATG5 and ATG7 caused SA-β-gal activity to be delayed but clearly senescence can occur even when autophagy is suppressed.

In conclusion, treatment of MCF-7 cells with either Adriamycin or Camptothecin induced both autophagy and senescence. Interference with ROS generation, ATM activation and induction of p52 or p21 suppressed both autophagy and senescence. However, these observations may indicate only that both responses are mediated by common DNA-damage induced signaling

pathways (that are also associated with conventional growth arrest). When autophagy was blocked either pharmacologically or genetically, senescence was temporally delayed, but *the overall extent of senescence induced by Adriamycin and Camptothecin was not attenuated.* Consequently, although autophagy appears to accelerate and facilitate the senescence process, likely by providing an additional source of energy to allow the cells to enter a prolonged dormant-like state, it is clear that senescence can occur independently of autophagy. It is furthermore increasingly becoming recognized that both autophagy and senescence are likely to play central roles in signaling to the immune system the presence of tumor cells that require elimination (Michaud et al., 2011; Ewald et al., 2010). Consequently the autophagy and senescence responses to chemotherapy are likely to have substantive involvement in mediating the complete elimination of tumors in response to chemotherapy.

Acknowledgements Electron microscopy was performed at the VCU Department of Anatomy and Neurobiology Microscopy Facility, supported, in part, with funding from the NIH-NINDS Center core grant 5P30NS047463. Quantification of β-galactosidase and acridine orange staining were conducted using the VCU Flow Cytometry and Imaging Shared Resource Facility. The RFP-LC3 vector was generously provided by Dr. Keith Miskimins at the University of South Dakota and was originally developed by the laboratory of Dr. A.M. Tolkovsky. The MCF7/ATG7$^{-/-}$ cells were a generous gift from the lab of Dr. Ameeta Kelekar at University of Minnesota, Minneapolis, MN. We would like to thank Drs. Kristopher Valerie, Sarah Golding and Amy Hawkins in the Department of Radiation Oncology at Virginia Commonwealth University for guidance with the studies relating to ATM signaling and silencing.

Authorship Contributions

Participated in Research Design: Goehe, Gewirtz, Valerie, Di

Conducted Experiments: Goehe, Di, Sharma, Bristol, Henderson

Contributed new reagents or analytic tools: Rodier, Davalos

Performed data analysis: Goehe, Di, Gewirtz, Henderson

Wrote or contributed to the writing of the manuscript: Goehe, Di, Gewirtz

References

Akbas SH, Timur M, and Ozben T (2005) The effect of quercetin on topotecan cytotoxicity in MCF-7 and MDA-MB 231 human breast cancer cells. *J Surg Res* **125**: 49-55.

Alexander A, Kim J, and Walker CL (2010) ATM engages the TSC2/mTORC1 signaling node to regulate autophagy. *Autophagy* **6**: 672-673.

Amaravadi RK, Yu D, Lum JJ, Bui T, Christophorou MA, Evan GI, Thomas-Tikhonenko A, and Thompson CB (2007) Autophagy inhibition enhances therapy-induced apoptosis in a Myc-induced model of lymphoma. *J Clin Invest* **117**: 326-36.

Azad MB, Chen Y, and Gibson SB (2009) Regulation of autophagy by reactive oxygen species (ROS): implications for cancer progression and treatment. *Antioxid Redox Signal* **11**: 777-790.

Bandhakavi S, Kim YM, Ro SH, Xie H, Onsongo G, Jun CB, Kim DH, and Griffin TJ (2010) Quantitative nuclear proteomics identifies mTOR regulation of DNA damage response. *Mol Cell Proteomics* **9**: 403-414.

Banin S, Moyal L, Shieh S, Taya Y, Anderson CW, Chessa L, Smorodinsky NI, Prives C, Reiss Y, Shiloh Y, and Ziv Y (1998) Enhanced phosphorylation of p53 by ATM in response to DNA damage. *Science* **281**:1674-1677.

Burma S, Chen BP, Murphy M, Kurimasa A, and Chen DJ (2001) ATM phosphorylates histone H2AX in response to DNA double-strand breaks. *J Biol Chem* **276**: 42462-42467.

Campisi, J. and d'Adda di Fagagna F (2007) Cellular senescence: when bad things happen to good cells. *Nat Rev Mol Cell Biol* **8**: 729-740.

Carew JS, Medina EC, Esquivel JA 2nd, Mahalingam D, Swords R, Kelly K, Zhang H, Huang P, Mita AC, Mita MM, Giles FJ, and Nawrocki ST (2010) Autophagy inhibition enhances vorinostat-induced apoptosis via ubiquitinated protein accumulation. *J Cell Mol Med* **14**: 2448-2459.

Chang BD, Xuan Y, Broude EV, Zhu H, Schott B, Fang J, and Roninson IB (1999) Role of p53 and p21waf1/cip1 in senescence-like terminal proliferation arrest induced in human tumor cells by chemotherapeutic drugs. *Oncogene* **18**: 4808-4818.

Colavitti, R. and Finkel T (2005) Reactive oxygen species as mediators of cellular senescence. *IUBMB Life* **57**: 277-281.

Crescenzi E, Palumbo G, de Boer J, and Brady HJ (2008) Ataxia telangiectasia mutated and p21CIP1 modulate cell survival of drug-induced senescent tumor cells: implications for chemotherapy. *Clin Cancer Res* **14**: 1877-1887.

d'Adda di Fagagna, F (2008) Living on a break: cellular senescence as a DNA-damage response. *Nat Rev Cancer* **8**: 512-522.

Debacq-Chainiaux F, Erusalimsky JD, Campisi J, and Toussaint O (2009) Protocols to detect senescence-associated beta-galactosidase (SA-betagal) activity, a biomarker of senescent cells in culture and in vivo. *Nat Protoc* **4**: 1798-1806.

Di X, Shiu RP, Newsham IF, and Gewirtz DA (2009) Apoptosis, autophagy, accelerated senescence and reactive oxygen in the response of human breast tumor cells to adriamycin. *Biochem Pharmacol* **77**: 1139-1150.

Di Micco R, Fumagalli M, Cicalese A, Piccinin S, Gasparini P, Luise C, Schurra C, Garre' M, Nuciforo PG, Bensimon A, Maestro R, Pelicci PG, and d'Adda di Fagagna F (2006) Oncogene-induced senescence is a DNA damage response triggered by DNA hyper-replication. *Nature* **444**: 638-642.

Elmore LW, Rehder CW, Di X, McChesney PA, Jackson-Cook CK, Gewirtz DA, and Holt SE (2002) Adriamycin-induced senescence in breast tumor cells involves functional p53 and telomere dysfunction. *J Biol Chem* **277**: 35509-35515.

Evan GI and d'Adda di Fagagna F (2009) Cellular senescence: hot or what? *Curr Opin Genet Dev* **19**: 25-31.

Ewald JA, Desotelle JA, Wilding G, and Jarrard DF (2010) Therapy-induced senescence in cancer. *J Natl Cancer Inst* **102**: 1536-1546.

Gerland LM, Peyrol S, Lallemand C, Branche R, Magaud JP,and Ffrench M (2003) Association of increased autophagic inclusions labeled for beta-galactosidase with fibroblastic aging. *Exp Gerontol* **38**: 887-895.

Gewirtz DA (2009) Autophagy, senescence and tumor dormancy in cancer therapy. *Autophagy* **5**: 1232-1234.

Gewirtz DA, Holt SE, and Elmore LW (2008) Accelerated senescence: an emerging role in tumor cell response to chemotherapy and radiation. *Biochem Pharmacol* **78**: 947-957.

Gewirtz DA, Hilliker ML, and Wilson EN (2009) Promotion of autophagy as a mechanism for radiation sensitization of breast tumor cells. *Radiother Oncol* **92**: 323-328.

Glick D, Barth S, and Macleod KF (2010) Autophagy: cellular and molecular mechanisms. *J Pathol* **221**: 3-12.

Gosselin K, Deruy E, Martien S, Vercamer C, Bouali F, Dujardin T, Slomianny C, Houel-Renault L, Chelli F, De Launoit Y, and Abbadie C (2009) Senescent keratinocytes die by autophagic programmed cell death. *Am J Pathol* **174**: 423-435.

Hickson I, Zhao Y, Richardson CJ, Green SJ, Martin NM, Orr AI, Reaper PM, Jackson SP, Curtin NJ, and Smith GC (2004) Identification and characterization of a novel and specific inhibitor of the ataxia-telangiectasia mutated kinase ATM. *Cancer Res* **64**: 9152-9159.

Jinno-Oue A, Shimizu N, Hamada N, Wada S, Tanaka A, Shinagawa M, Ohtsuki T, Mori T, Saha MN, Hoque AS, Islam S, Kogure K, Funayama T, Kobayashi Y, and Hoshino H (2010) Irradiation with carbon ion beams induces apoptosis, autophagy, and cellular senescence in a human glioma-derived cell line. *Int J Radiat Oncol Biol Phys* **76**: 229-241.

Karna P, Zughaier S, Pannu V, Simmons R, Narayan S, and Aneja R (2010) Induction of reactive oxygen species-mediated autophagy by a novel microtubule-modulating agent. *J Biol Chem* **285**: 18737-18748.

Kroemer G and Levine B (2008) Autophagic cell death: the story of a misnomer. *Nat Rev Mol Cell Biol* **9**: 1004-10010.

Komatsu M, Waguri S, Ueno T, Iwata J, Murata S, Tanida I, Ezaki J, Mizushima N, Ohsumi Y, Uchiyama Y, Kominami E, Tanaka K, and Chiba T (2005) Impairment of starvation-induced and constitutive autophagy in Atg7-deficient mice. *J Cell Biol* **169**: 425-434.

Kuilman T, Michaloglou C, Mooi WJ, and Peeper DS (2010) The essence of senescence. *Genes Dev* **24**: 2463-2479.

Kuma A, Mizushima N, Ishihara N, and Ohsumi Y (2002) Formation of the approximately 350-kDa Apg12-Apg5.Apg16 multimeric complex, mediated by Apg16 oligomerization, is essential for autophagy in yeast. *J Biol Chem* **277**: 18619-18625.

Kurz EU, Douglas P, and Lees-Miller SP (2004) Doxorubicin activates ATM-dependent phosphorylation of multiple downstream targets in part through the generation of reactive oxygen species. *J Biol Chem* **279**: 53272-53281.

Lee H, Kwak HJ, Cho IT, Park SH, and Lee CH (2009) S1219 residue of 53BP1 is phosphorylated by ATM kinase upon DNA damage and required for proper execution of DNA damage response. *Biochem Biophys Res Commun* **378**: 32-36.

Lee AC, Fenster BE, Ito H, Takeda K, Bae NS, Hirai T, Yu ZX, Ferrans VJ, Howard BH, and Finkel T (1999) Ras proteins induce senescence by altering the intracellular levels of reactive oxygen species. *J Biol Chem* **274**: 7936-7940.

Lin CI, Whang EE, Abramson MA, Jiang X, Price BD, Donner DB, Moore FD Jr, and Ruan DT (2009) Autophagy: a new target for advanced papillary thyroid cancer therapy. *Surgery* **146**: 1208-1214.

Lu Z, Luo RZ, Lu Y, Zhang X, Yu Q, Khare S, Kondo S, Kondo Y, Yu Y, Mills GB, Liao WS, and Bast RC Jr (2008) The tumor suppressor gene ARHI regulates autophagy and tumor dormancy in human ovarian cancer cells. *J Clin Invest* **118**: 3917-3929.

Luo Y, Zou P, Zou J, Wang J, Zhou D, and Liu L (2010) Autophagy regulates ROS-induced cellular senescence via p21 in a p38 MAPKalpha dependent manner. *Exp Gerontol* **46**: 860-867.

Macip S, Igarashi M, Fang L, Chen A, Pan ZQ, Lee SW, and Aaronson SA (2002) Inhibition of p21-mediated ROS accumulation can rescue p21-induced senescence. *EMBO J* **21**: 2180-2188.

Mallette FA, Gaumont-Leclerc MF, and Ferbeyre G (2007) The DNA damage signaling pathway is a critical mediator of oncogene-induced senescence. *Genes Dev* **21**: 43-48.

Michaud M, Martins I, Sukkurwala AQ, Adjemian S, Ma Y, Pellegatti P, Shen S, Kepp O, Scoazec M, Mignot G, Rello-Varona S, Tailler M, Menger L, Vacchelli E, Galluzzi L, Ghiringhelli F, di Virgilio F, Zitvogel L, and Kroemer G (2011) Autophagy-dependent anticancer immune responses induced by chemotherapeutic agents in mice. *Science* **334**: 1573-1577.

Mizushima N, Yoshimori T, and Levine B (2010) Methods in mammalian autophagy research. *Cell* **140**: 313-326.

Notte A, Leclere L, and Michiels C (2011) Autophagy as a mediator of chemotherapy-induced cell death in cancer. *Biochem Pharmacol* **82**: 427-434.

Pankiv S, Clausen TH, Lamark T, Brech A, Bruun JA, Outzen H, Øvervatn A, Bjørkøy G, and Johansen T (2007) p62/SQSTM1 binds directly to Atg8/LC3 to facilitate degradation of ubiquitinated protein aggregates by autophagy. *J Biol Chem* **282**: 24131-24145.

Patschan S, Chen J, Polotskaia A, Mendelev N, Cheng J, Patschan D, and Goligorsky MS (2008) Lipid mediators of autophagy in stress-induced premature senescence of endothelial cells. *Am J Physiol Heart Circ Physiol* **294**: H1119-H1129.

Petiot A, Ogier-Denis E, Blommaart EF, Meijer AJ, and Codogno P (2000) Distinct classes of phosphatidylinositol 3'-kinases are involved in signaling pathways that control macroautophagy in HT-29 cells. *J Biol Chem* **275**: 992-998.

Probin V, Wang Y, and Zhou D (2007) Busulfan-induced senescence is dependent on ROS production upstream of the MAPK pathway. *Free Radic Biol Med* **42**: 1858-18565.

Qian H and Yang Y (2009) Alterations of cellular organelles in human liver-derived hepatoma G2 cells induced by adriamycin. *Anticancer Drugs* **20**: 779-786.

Ravizza R, Gariboldi MB, Passarelli L, and Monti E. Role of the p53/p21 system in the response of human colon carcinoma cells to Doxorubicin. *BMC Cancer* **4**: 92-100.

Roninson IB (2002) Oncogenic functions of tumour suppressor p21(Waf1/Cip1/Sdi1): association with cell senescence and tumour-promoting activities of stromal fibroblasts. Cancer Lett 17: 1-14.

Roninson IB (2003) Tumor cell senescence in cancer treatment. *Cancer Res* **63**: 2705-2715.

Sasaki M, Miyakoshi M, Sato Y, and Nakanuma Y (2010) Autophagy mediates the process of cellular senescence characterizing bile duct damages in primary biliary cirrhosis. *Lab Invest* **90**: 835-843.

Seibenhener ML, Babu JR, Geetha T, Wong HC, Krishna NR, and Wooten MW (2004) Sequestosome 1/p62 is a polyubiquitin chain binding protein involved in ubiquitin proteasome degradation. *Mol Cell Biol* **24**: 8055-8068.

Shay JW and Roninson IB (2004) Hallmarks of senescence in carcinogenesis and cancer therapy. *Oncogene* **23**: 2919-2933.

Somasundaram S, Edmund NA, Moore DT, Small GW, Shi YY, and Orlowski RZ (2002) Dietary curcumin inhibits chemotherapy-induced apoptosis in models of human breast cancer. *Cancer Res* **62**: 3868-3875.

Song YS, Lee BY, and Hwang ES (2005) Dinstinct ROS and biochemical profiles in cells undergoing DNA damage-induced senescence and apoptosis. *Mech Ageing Dev* **126**: 580-590.

Su D, Zhu S, Han X, Feng Y, Huang H, Ren G, Pan L, Zhang Y, Lu J, and Huang B (2009) BMP4-Smad signaling pathway mediates adriamycin-induced premature senescence in lung cancer cells. *J Biol Chem* **284**: 12153-12164.

Thorburn A (2008) Apoptosis and autophagy: regulatory connections between two supposedly different processes. *Apoptosis* **13**: 1-9.

Wang H, Zhao Y, Li L, McNutt MA, Wu L, Lu S, Yu Y, Zhou W, Feng J, Chai G, Yang Y, and Zhu WG (2008) An ATM- and Rad3-related (ATR) signaling pathway and a phosphorylation-acetylation cascade are involved in activation of p53/p21Waf1/Cip1 in response to 5-aza-2'-deoxycytidine treatment. *J Biol Chem* **283**: 2564-2574.

Xi G, Hu X, Wu B, Jiang H, Young CY, Pang Y, and Yuan H (2011) Autophagy inhibition promotes paclitaxel-induced apoptosis in cancer cells. *Cancer Lett* **307**: 141-148.

Young AR, Narita M, Ferreira M, Kirschner K, Sadaie M, Darot JF, Tavaré S, Arakawa S, Shimizu S, Watt FM, Narita M (2009) Autophagy mediates the mitotic senescence transition. *Genes Dev* **23**: 798-803.

Zhan H, Suzuki T, Aizawa K, Miyagawa K, and Nagai R (2010) Ataxia telangiectasia mutated (ATM)-mediated DNA damage response in oxidative stress-induced vascular endothelial cell senescence. *J Biol Chem* **285**: 29662-29670.

Footnotes

Rachel W. Goehe and Xu Di contributed equally to the manuscript.

The VCU Flow Cytometry and Imaging Shared Resource Facility is supported in part by Flow Cytometry Core grant, [National Institutes of Health Grant P30CA16059]. Dr. Goehe was supported by [National Institutes of Health Grant T32 CA113277-04].

JPET Fast Forward. Published on August 27, 2012 as DOI: 10.1124/jpet.112.197590
This article has not been copyedited and formatted. The final version may differ from this version.

Legends for Figures

Figure 1. Adriamycin (ADR) induces both senescence and autophagy in MCF-7 cells. MCF-7 cells were treated with 1μM ADR for 2 h followed by drug removal and replacement with fresh medium. **A)** β-galactosidase staining. Control cells generally show minimal staining. **B)** *Left Panel:* Representative histogram of positive C_{12}FDG fluorescent cells for each treatment. *Right Panel:* Flow cytometric detection of SA-β-gal activity as measured by C_{12}FDG-fluorescin fluorescence. *p<0.001 compared to control. **C)** Cells were stained with acridine orange (AOS) and imaged by fluorescence microscopy. **D)** *Left Panel*: Representative dot plots of positive acridine orange staining for each treatment. *Right Panel:* Cells were quantified for AVO formation produced by ADR treatment by FACS analysis. *p<0.001 compared to control. **E)** Punctuate signal of RFP-LC3 and transmission electron microscopy imaging after 72 h post ADR treatment. Arrowheads in red indicate autophagosome formation. **F)** Immunoblot analysis of p62, p21, pRB, and ß-actin. Data are representative of an average of three independent experiments.

Figure 2. Involvement of free radicals in ADR-induced senescence and autophagy. MCF-7 cells were pretreated with 20μM of glutathione (GSH) or 20μM N-acetyl cysteine (NAC) for 1 h followed by 1μM of ADR for 2 h. The drugs were removed and fresh media was restored. **A)** Senescence was evaluated by β-galactosidase staining 72 h post treatment (Left Panel) and quantified for C_{12}FDG-fluorescin fluorescence by FACS analysis (Right Panel) *p < 0.001 compared to control. **B)** Immunoblot analysis of p53, p21, pRb, and β-actin. **C)** Acridine orange staining visualized by fluorescence microscopy (Upper Panel) and quantified by FACS analysis (Lower Panel). #p <0.05 compared to ADR treatment on Day 3 and *p < 0.001 compared to ADR treatment on Day 5. **D)** Immunoblot analysis of p62 and β-actin were evaluated 72 h post treatment. **E)** Fluorescence microscopy for RFP-LC3 at 72 h after initiation of the indicated treatments.

Figure 3. Influence of ATM activity on ADR-induced senescence and autophagy. MCF-7 cells were treated with 1μM ADR for 2 h preceded by a 2 hr exposure to 20μM KU55933 or 2mM caffeine. **A)** *Upper Panel:* MCF-7 cells were fixed and stained for β-Galactosidase. *Lower Panel:* Flow cytometric detection of SA-β-gal activity as measured by C_{12}FDG-fluorescin fluorescence. *p<0.001 compared to ADR treatment. **B)** Immunoblot analysis of p53, p21, pRb,

JPET Fast Forward. Published on August 27, 2012 as DOI: 10.1124/jpet.112.197590
This article has not been copyedited and formatted. The final version may differ from this version.

and β-actin. **C)** Acridine orange staining visualized by fluorescence microscopy. **D)** *Left Panel:* Representative dot plots of positive acridine orange staining for each of the indicated treatment. *Right Panel:* Quantification of acridine orange staining by FACS analysis. *p<0.001 compared to ADR and #p<0.003 compared to ADR. **E)** Immunoblot analyses of p62 and ß-actin. **F-G)** MCF-7 cells were transfected with either shRNA against a scramble control (shCON) or shRNA against ATM (shATM). **F)** shCON and shATM MCF-7 cells were assessed for β-galactosidase staining 72 h post ADR treatment. **G)** Cells with AVO formation were monitored by FACS analysis 72 h post treatment. *p<0.001 compared to shCON + ADR.

Figure 4. Downregulation of p21 attenuates ADR-induced autophagy. MCF-7 cells were stably infected with either shRNA against a scramble control (shCON) or shRNA against p21 (shp21). Cell lines were treated with 1μM ADR for 2 h, which was then replaced with complete medium. **A)** Immunoblot analyses of lysates from shCON and shp21 cells treated with or without ADR for 72 h. **B)** Cells were stained with β-galactosidase, and images were taken 72h post ADR treatment (Left Panel) and quantified for C_{12}FDG-fluorescin fluorescence by FACS analysis (Right Panel). *p<0.05 compared to shCON + ADR. **C)** *Upper Panel:* Acridine orange images were taken at 72 h post ADR treatment. *Lower Panel:* Cells with AVO formation were monitored by FACS analysis 72 h post treatment. *p<0.003 compared to shCON + ADR.

Figure 5. Impact of autophagic inhibitors on ADR-induced senescence. MCF-7 cells were pretreated with 5mM of 3-MA or 5μM of chloroquine for 1 h followed by 1μM of ADR for 2 h. ADR was removed and fresh media was restored with or without 3-MA or chloroquine. **A)** *Upper Panel:* Acridine orange images were taken at 72 h post ADR treatment. *Lower Panel:* Cells with AVO formation were monitored by FACS analysis 72 h post treatment. *p<0.001 compared to ADR. **B)** Immunoblot analysis of p62 and ß-actin. **C)** Cells were stained with β-galactosidase, and images were taken at the indicated times post ADR treatment. **D)** Immunoblot analysis of p21, p53, and ß-actin.

Figure 6. Genetic silencing of ATG5 temporarily delayed ADR-induced senescence. MCF-7 cells were stably infected with either shRNA against a scramble control (shCON) or shRNA against ATG5 (shATG5). Cell lines were treated with 1μM ADR for 2h, which was then replaced with complete medium. **A)** Immunoblot analyses of lysates from shCON and shATG5 cells treated with or without ADR for 72 h for ATG5 and β-actin. **B)** Acridine orange staining

JPET Fast Forward. Published on August 27, 2012 as DOI: 10.1124/jpet.112.197590
This article has not been copyedited and formatted. The final version may differ from this version.

visualized by fluorescence microscopy (Upper Panel) and quantified by FACS analysis (Lower Panel). *p<0.001 compared to shCON + ADR Day 3 and shCON + ADR Day 5. #p<0.05 compared to ADR Day 1. **C)** β-Galactosidase staining (Upper Panel) and flow cytometric detection of SA-β-gal activity as measured by C_{12}FDG-fluorescin fluorescence.

Figure 7. Genetic silencing of ATG5 temporarily delayed ADR-induced senescence. MCF-7 cells were stably infected with either shRNA against a scramble control (shCON) or shRNA against ATG7 (shATG7). Cell lines were treated with 1μM ADR for 2 h, which was then replaced with complete medium. **A)** Immunoblot analyses of lysates from shCON and shATG5 cells treated with or without ADR for 72 h for ATG5 and β-actin. **B)** Acridine orange staining visualized by fluorescence microscopy (*Upper Panel*) and quantified by FACS analysis (*Lower Panel*). *p<0.001 compared to shCON + ADR Day 3 and shCON + ADR Day 5. **C)** Immunoblot analyses of lysates from shCON and shATG7 cells treated with or without ADR for 72 h for p62 and β-actin. **D)** β-galactosidase staining (*Upper Panel*) and flow cytometric detection of SA-β-gal activity as measured by C_{12}FDG-fluorescin fluorescence (*Lower Panel)*. **E)** Immunoblot analysis of p21 and ß-actin.

Figure 8. Silencing autophagy temporarily delayed CPT-induced senescence. MCF-7 cells were treated with 5μM of CPT for 2 h followed by drug removal and replacement with fresh medium. **A)** β-galactosidase staining. **B)** *Left Panel:* Representative histograms of positive C_{12}FDG fluorescent cells for each treatment. *Right Panel:* Flow cytometric detection of SA-β-gal activity as measured by C_{12}FDG-fluorescin fluorescence. *p<0.001 compared to control. **C)** Cells were stained with acridine orange (AOS) and imaged by fluorescence microscopy. **D)** *Left Panel*: Representative dot plots of positive acridine orange staining for each treatment. *Right Panel:* Cells were quantified for AVO formation produced by CPT treatment by FACS analysis. *p<0.001 compared to control. **E)** Acridine orange staining of CPT treated MCF-7 cells at the indicated timepoints (Upper Panel) and quantification of AVO formation by FACS analysis (Lower Panel). *p<0.001 compared to shCON + CPT Day 3 and shCON + CPT Day 5. #p<0.05 compared to shCON + CPT Day 1. **F)** β-galactosidase staining of CPT treated MCF-7 cells at the indicated timepoints (Upper Panel) and quantification of C_{12}FDG-fluorescin fluorescence by FACS analysis (Lower Panel). **G)** Immunoblot analysis of p62 and ß-actin.

JPET Fast Forward. Published on August 27, 2012 as DOI: 10.1124/jpet.112.197590
This article has not been copyedited and formatted. The final version may differ from this version.

A

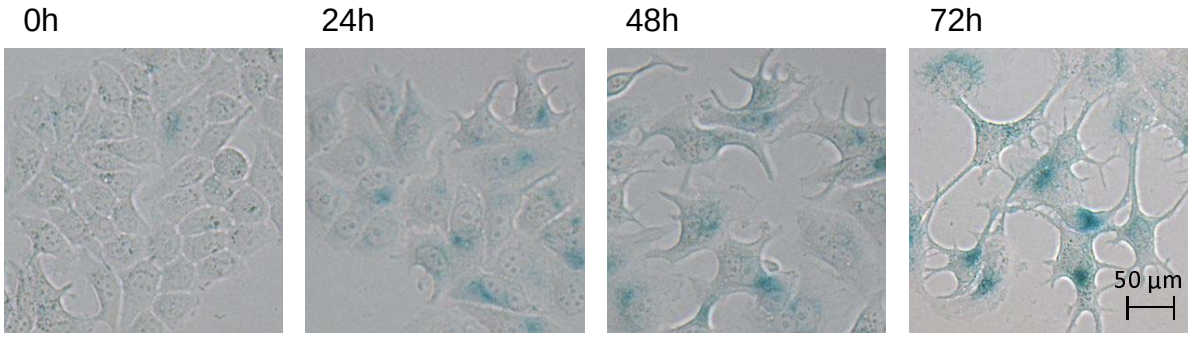

B

Left Panel

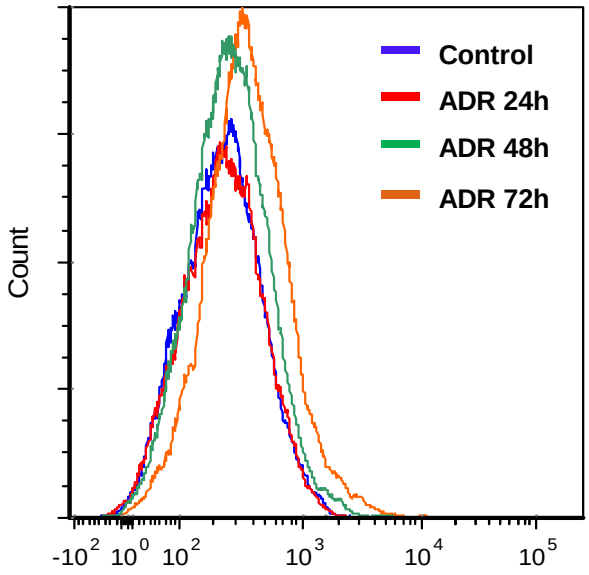

Right Panel

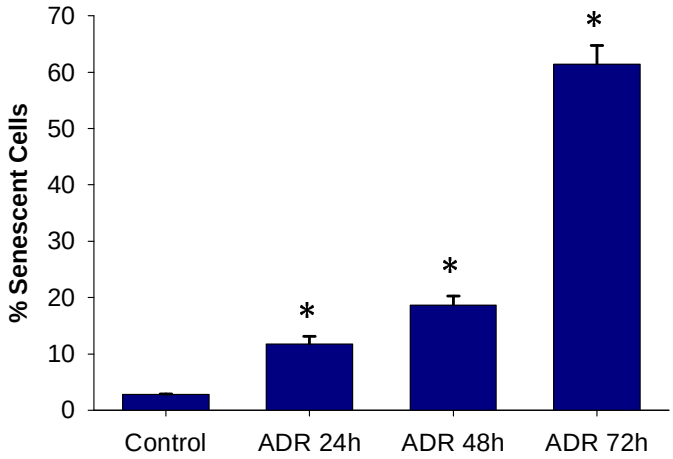

Figure 1

JPET Fast Forward. Published on August 27, 2012 as DOI: 10.1124/jpet.112.197590
This article has not been copyedited and formatted. The final version may differ from this version.

C

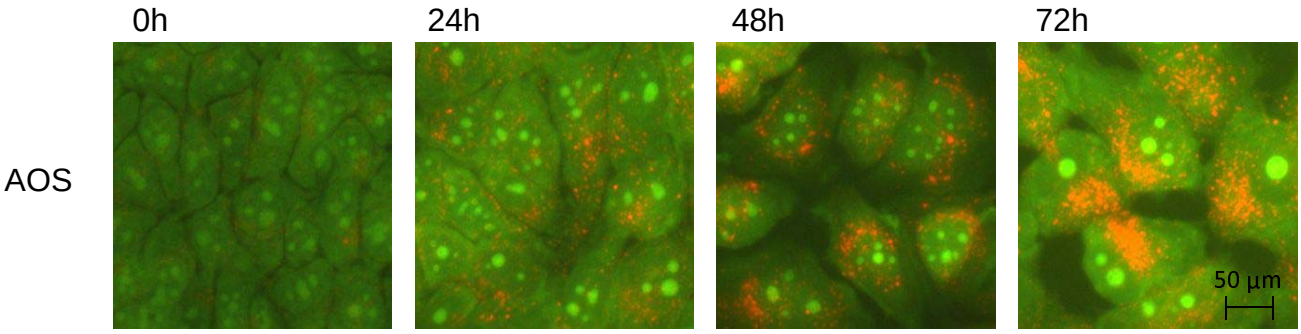

D

Left Panel

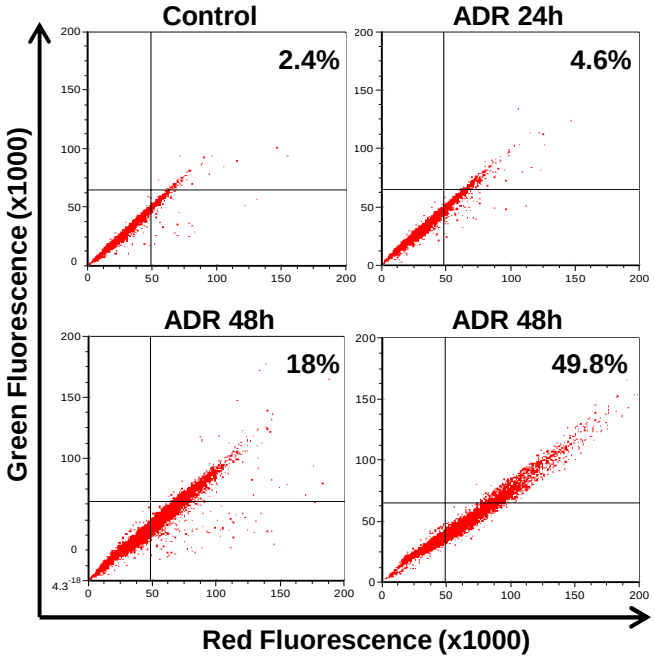

Right Panel

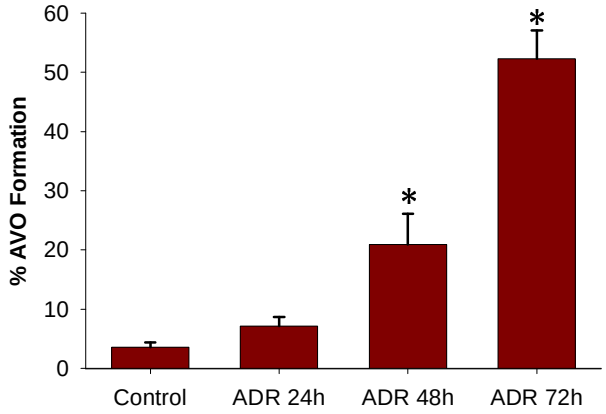

Figure 1

JPET Fast Forward. Published on August 27, 2012 as DOI: 10.1124/jpet.112.197590
This article has not been copyedited and formatted. The final version may differ from this version.

E

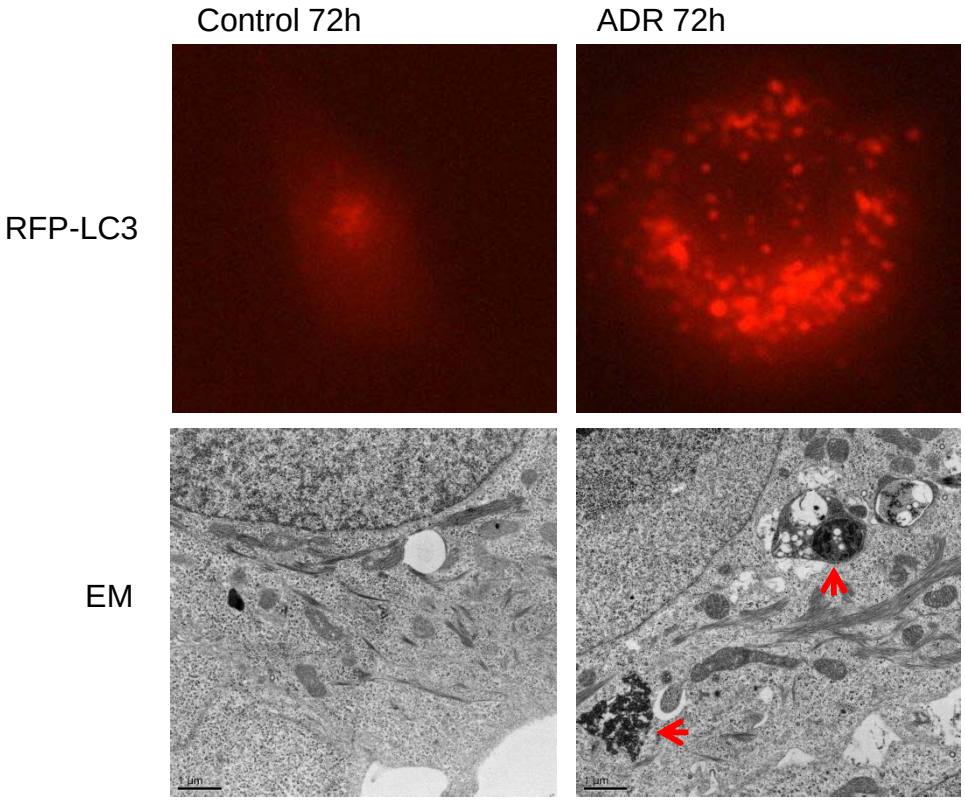

F

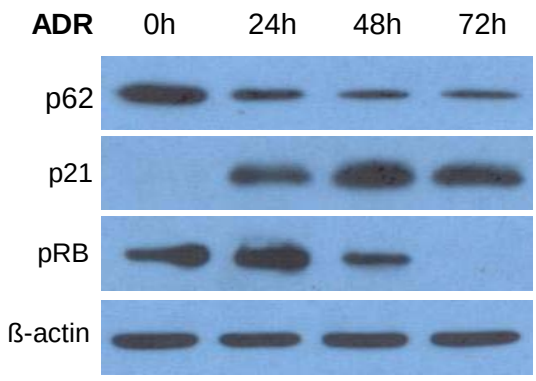

Figure 1

JPET Fast Forward. Published on August 27, 2012 as DOI: 10.1124/jpet.112.197590
This article has not been copyedited and formatted. The final version may differ from this version.

A

Left Panel

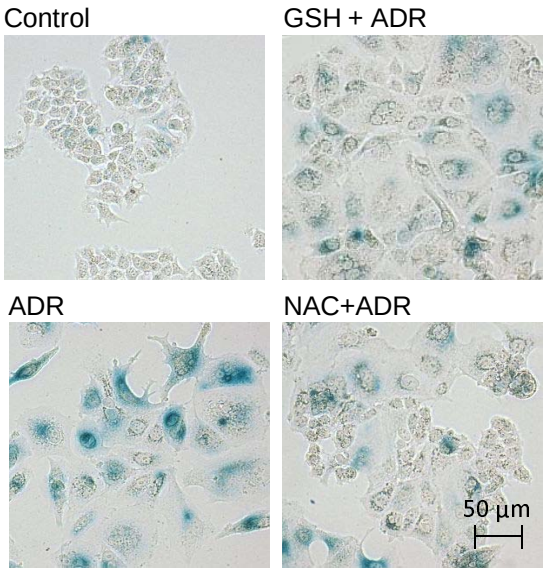

Right Panel

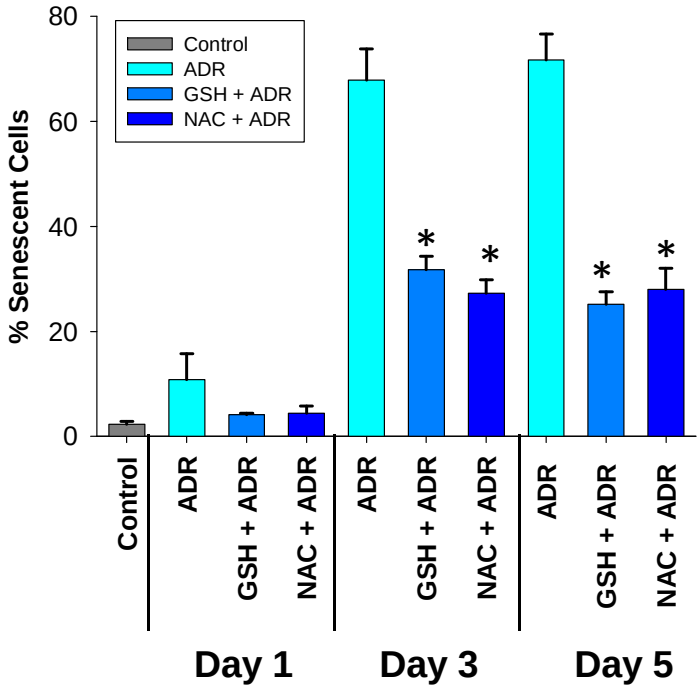

B

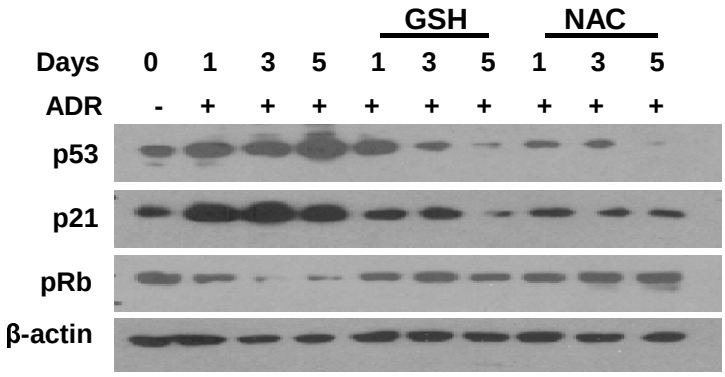

Figure 2

JPET Fast Forward. Published on August 27, 2012 as DOI: 10.1124/jpet.112.197590
This article has not been copyedited and formatted. The final version may differ from this version.

C

Upper Panel

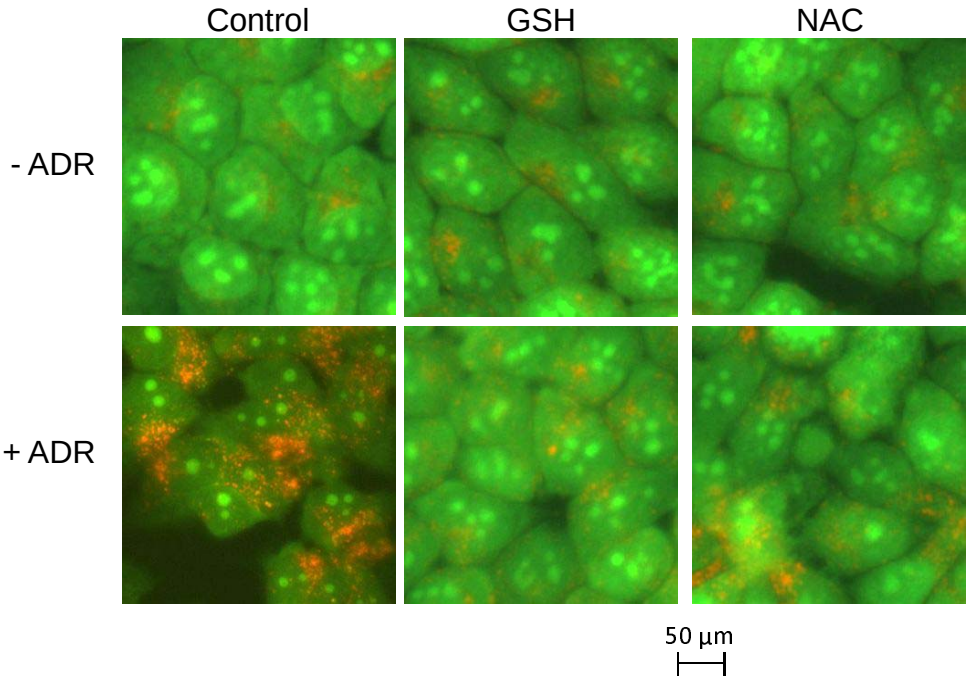

Lower Panel

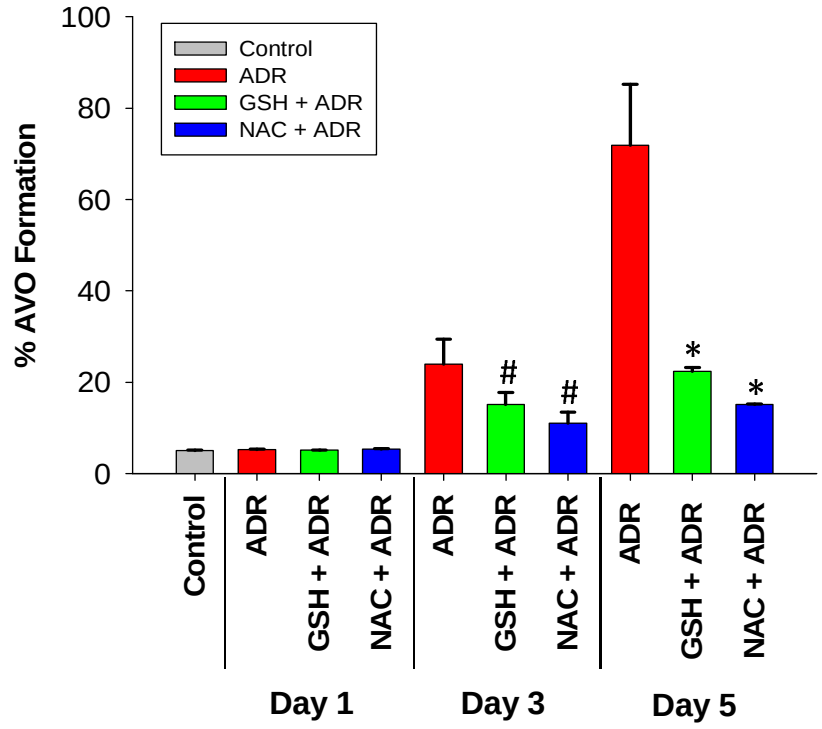

Figure 2

JPET Fast Forward. Published on August 27, 2012 as DOI: 10.1124/jpet.112.197590
This article has not been copyedited and formatted. The final version may differ from this version.

D

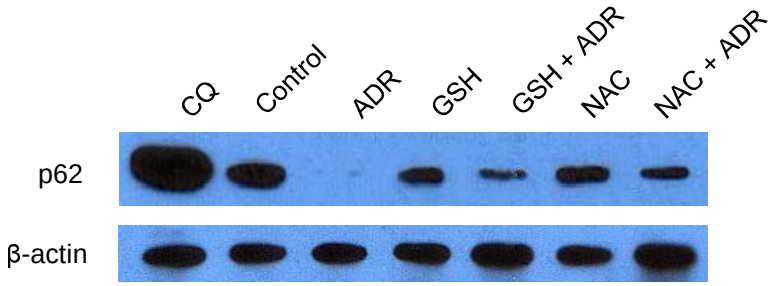

E

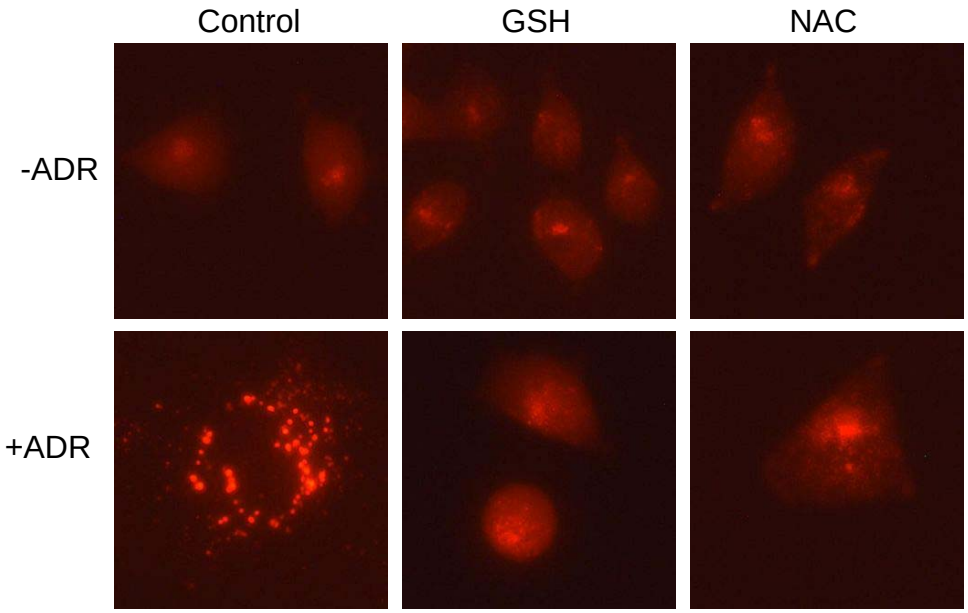

Figure 2

JPET Fast Forward. Published on August 27, 2012 as DOI: 10.1124/jpet.112.197590
This article has not been copyedited and formatted. The final version may differ from this version.

A

Upper Panel

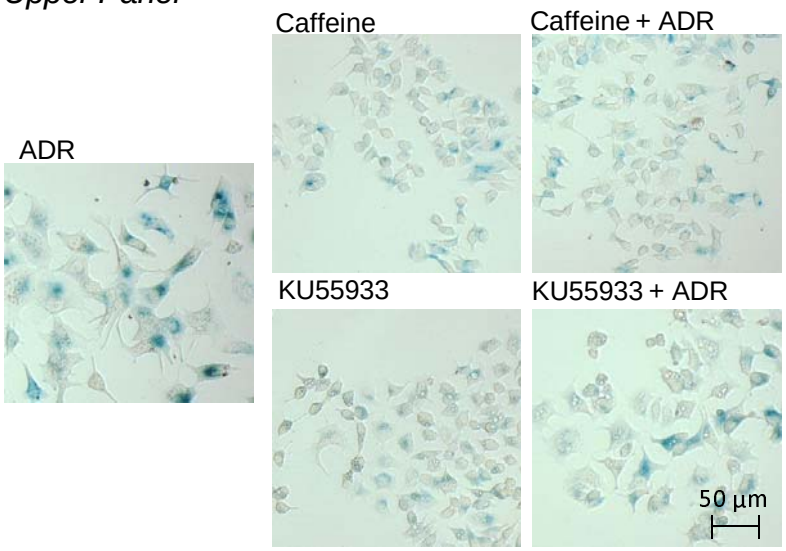

Lower Panel

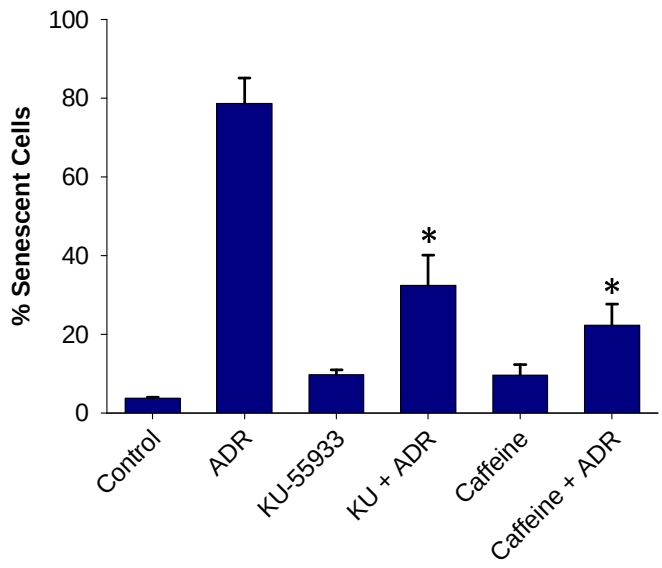

B

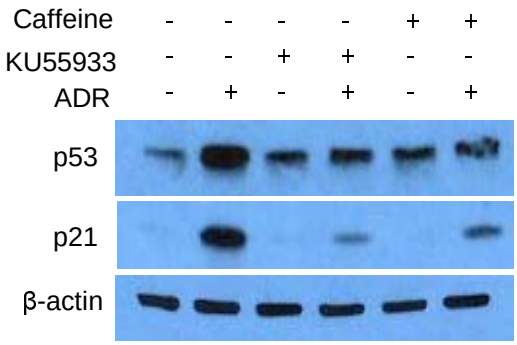

Figure 3

JPET Fast Forward. Published on August 27, 2012 as DOI: 10.1124/jpet.112.197590
This article has not been copyedited and formatted. The final version may differ from this version.

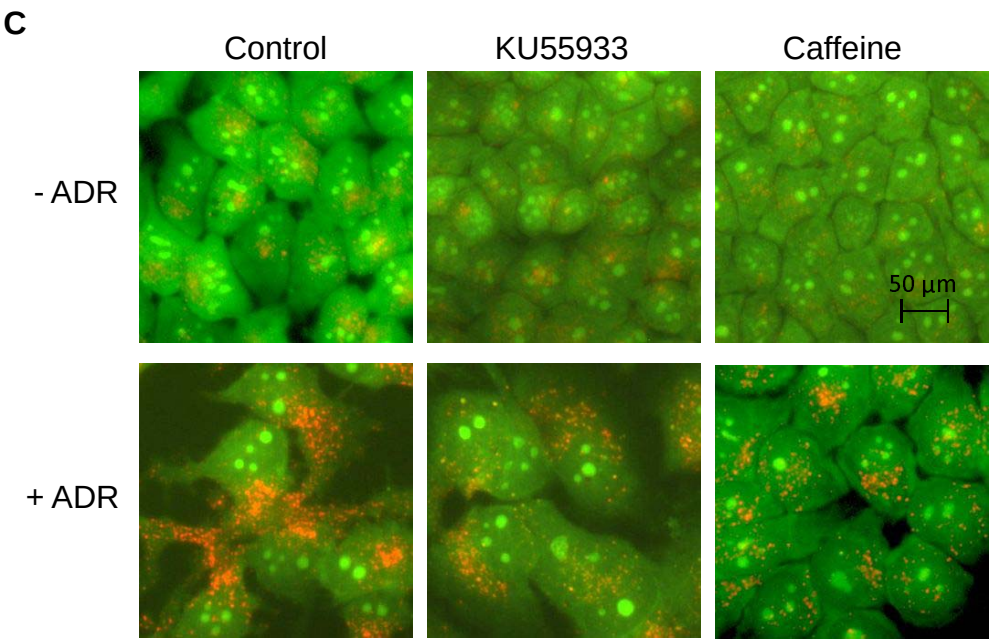

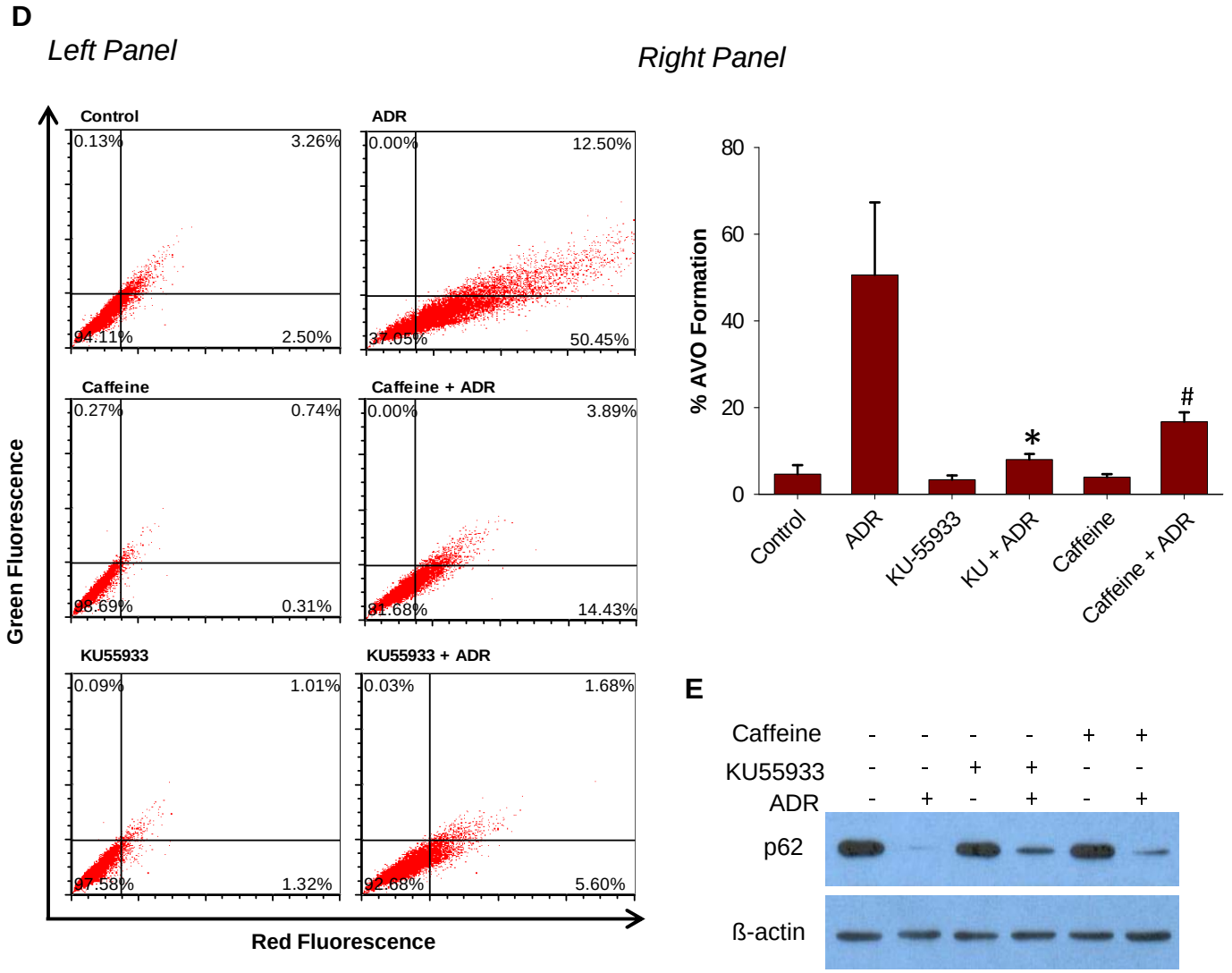

Figure 3

JPET Fast Forward. Published on August 27, 2012 as DOI: 10.1124/jpet.112.197590
This article has not been copyedited and formatted. The final version may differ from this version.

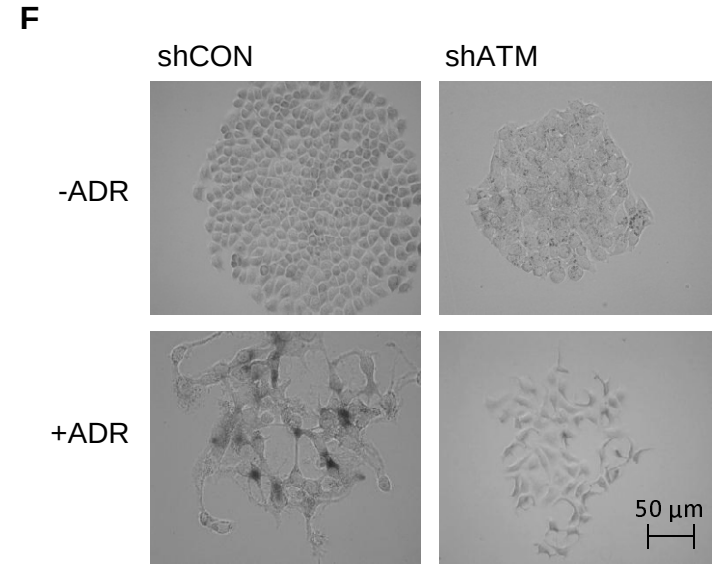

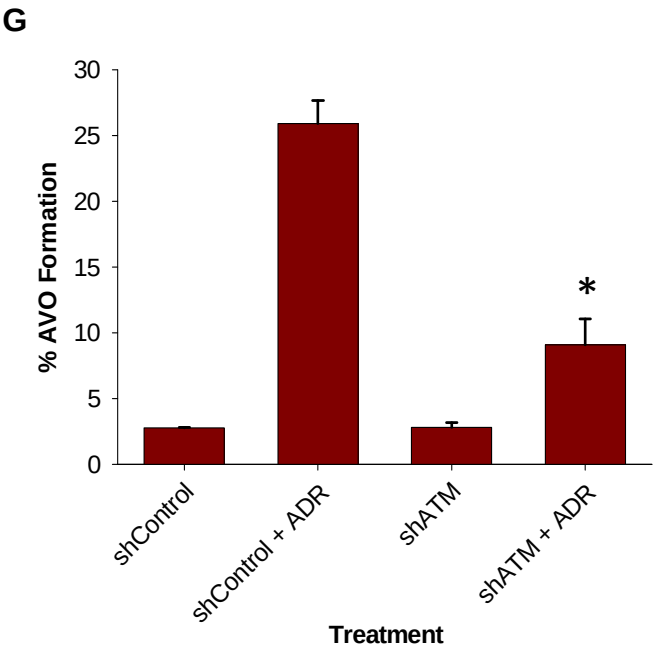

Figure 3

JPET Fast Forward. Published on August 27, 2012 as DOI: 10.1124/jpet.112.197590
This article has not been copyedited and formatted. The final version may differ from this version.

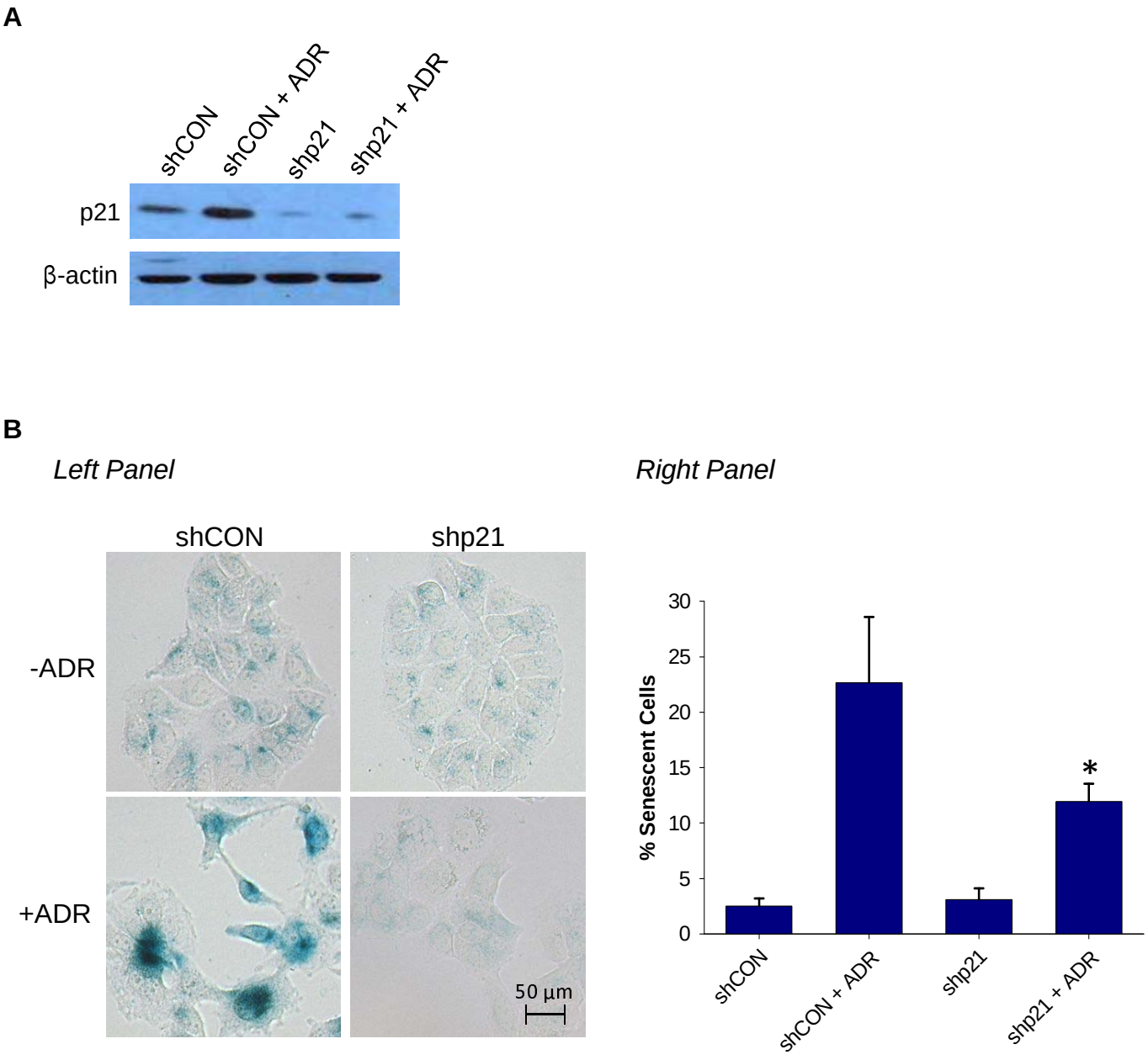

Figure 4

JPET Fast Forward. Published on August 27, 2012 as DOI: 10.1124/jpet.112.197590
This article has not been copyedited and formatted. The final version may differ from this version.

C

Upper Panel

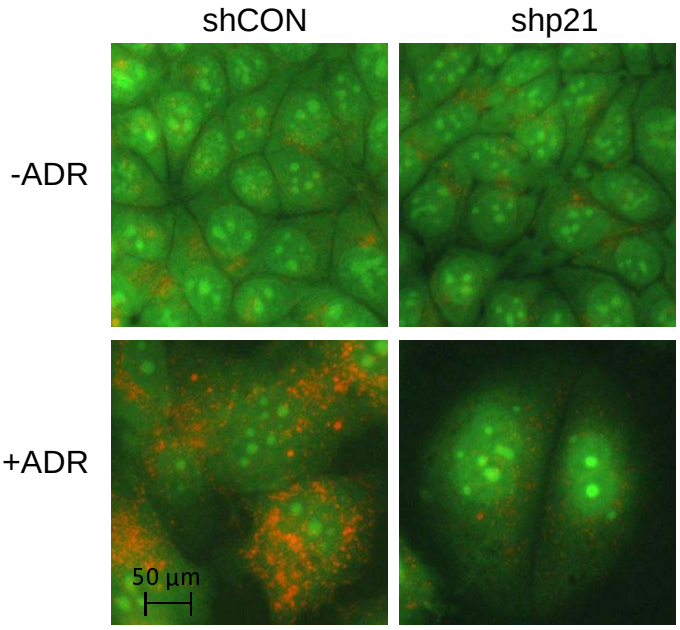

Lower Panel

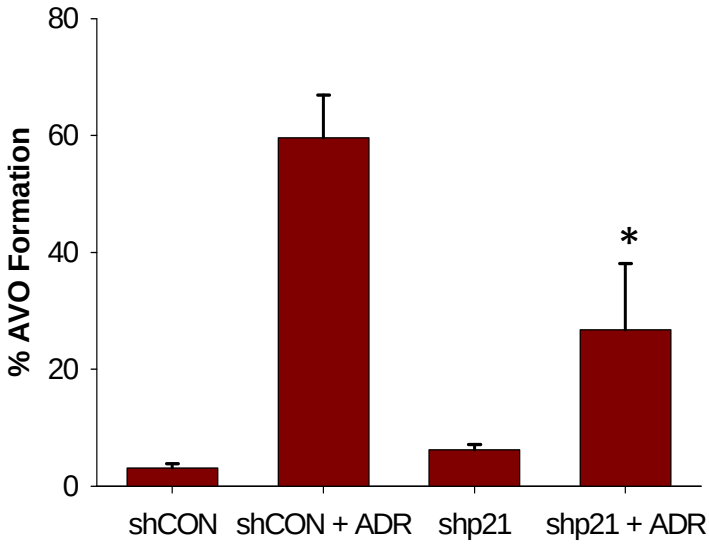

Figure 4

JPET Fast Forward. Published on August 27, 2012 as DOI: 10.1124/jpet.112.197590
This article has not been copyedited and formatted. The final version may differ from this version.

A

Upper Panel

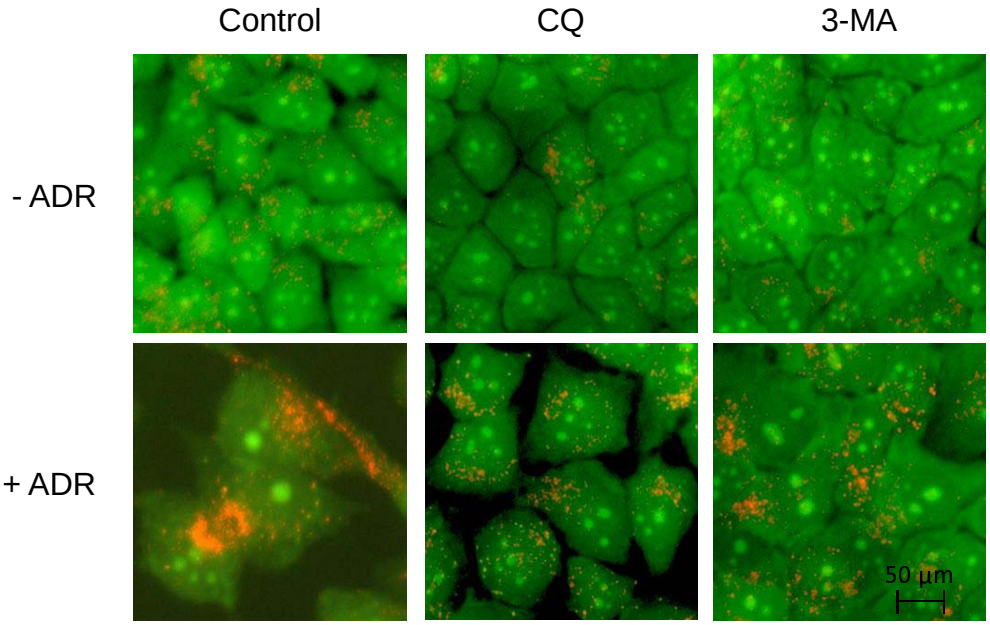

Lower Panel

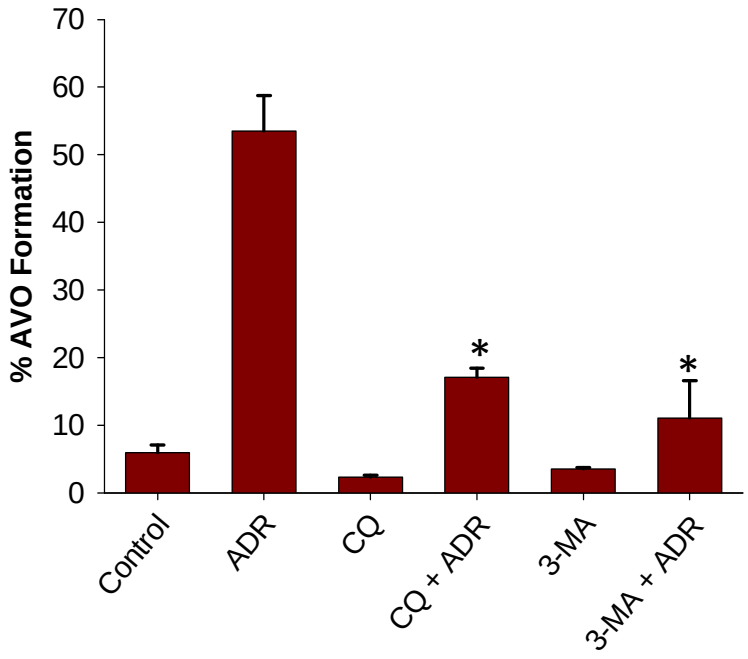

Figure 5

JPET Fast Forward. Published on August 27, 2012 as DOI: 10.1124/jpet.112.197590
This article has not been copyedited and formatted. The final version may differ from this version.

B

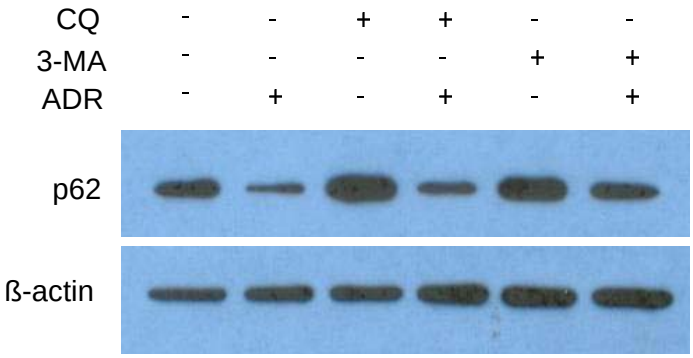

C

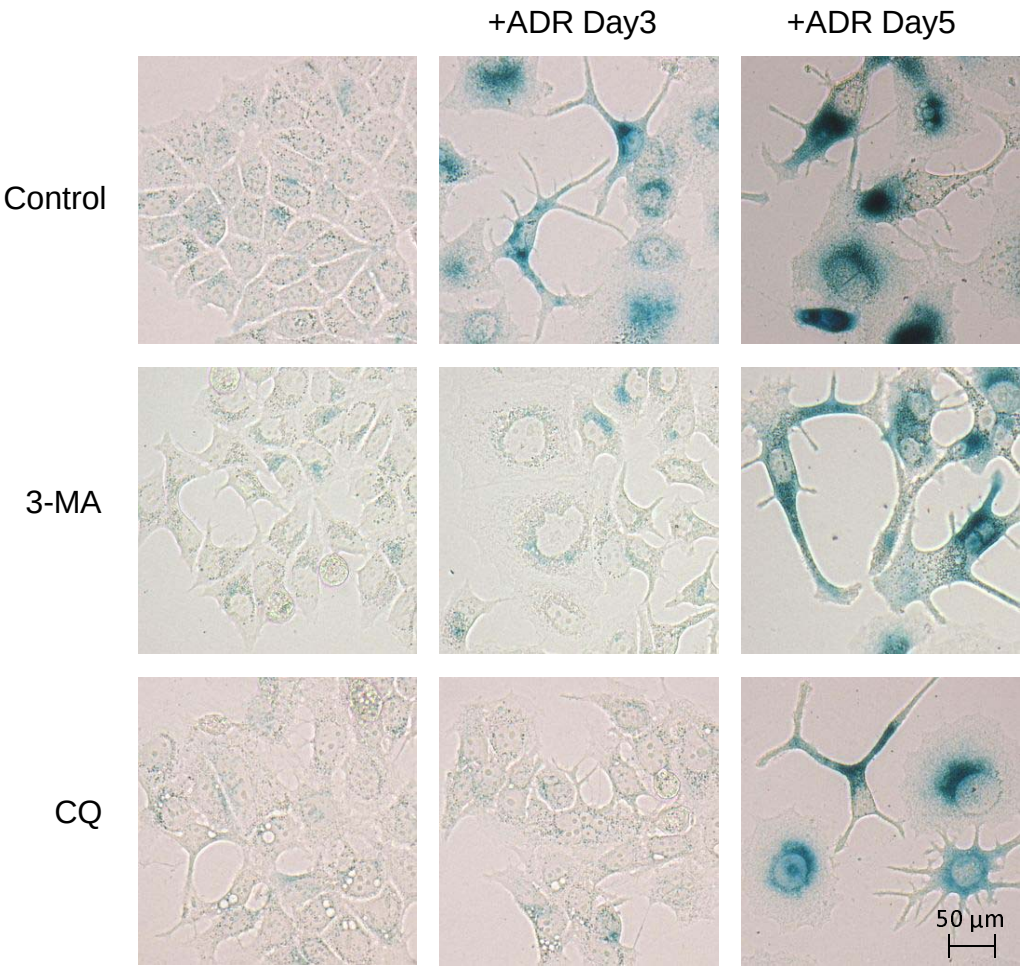

Figure 5

JPET Fast Forward. Published on August 27, 2012 as DOI: 10.1124/jpet.112.197590
This article has not been copyedited and formatted. The final version may differ from this version.

D

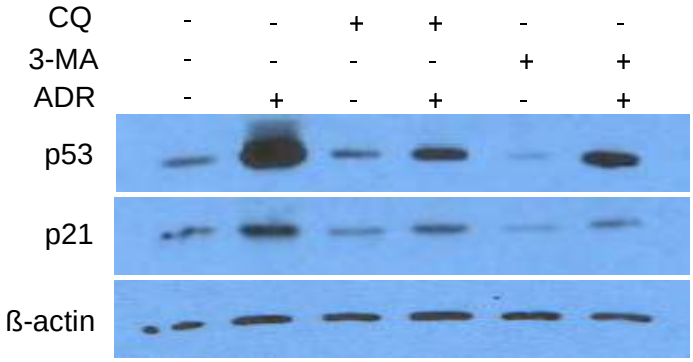

Figure 5

JPET Fast Forward. Published on August 27, 2012 as DOI: 10.1124/jpet.112.197590
This article has not been copyedited and formatted. The final version may differ from this version.

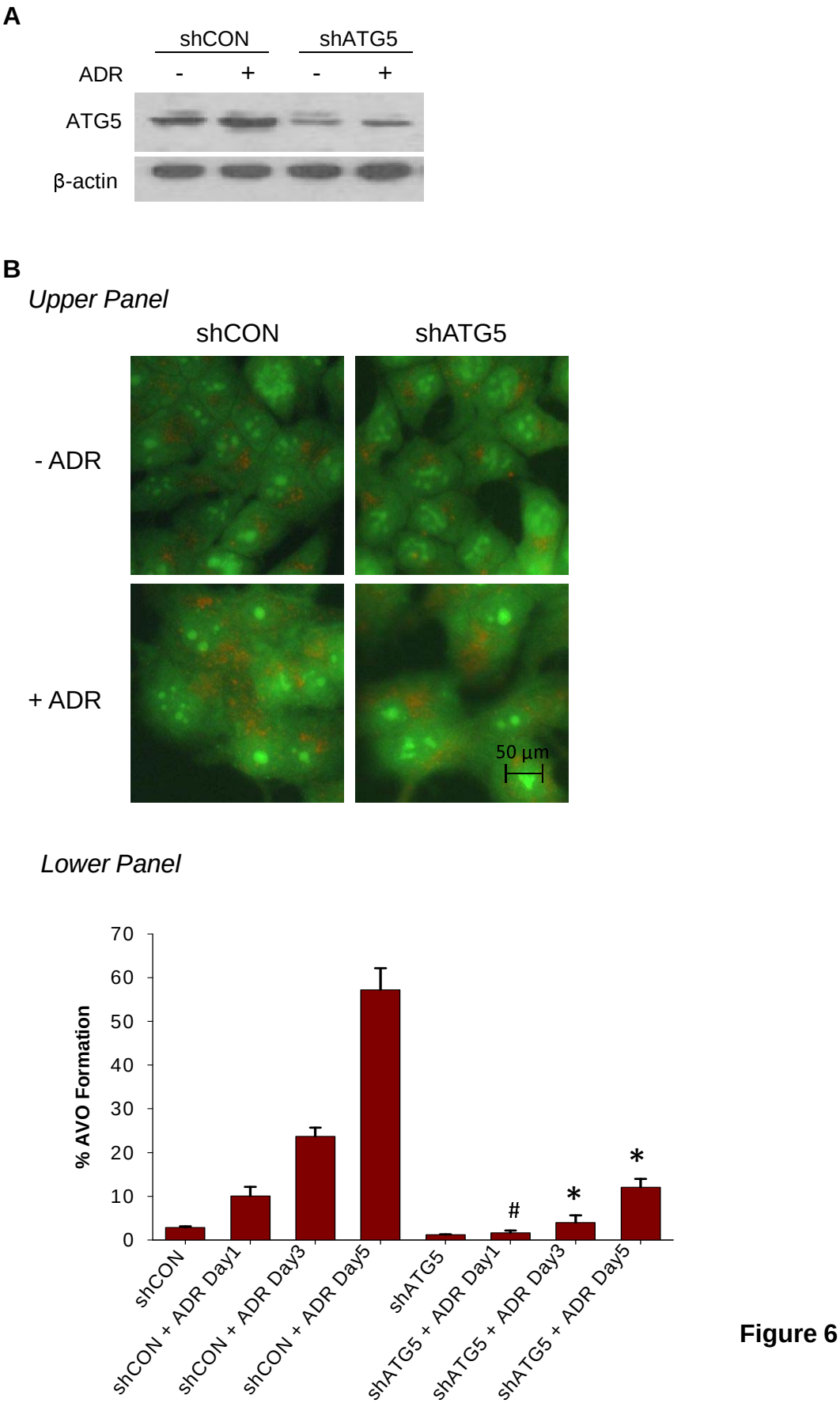

Figure 6

JPET Fast Forward. Published on August 27, 2012 as DOI: 10.1124/jpet.112.197590
This article has not been copyedited and formatted. The final version may differ from this version.

C

Upper Panel

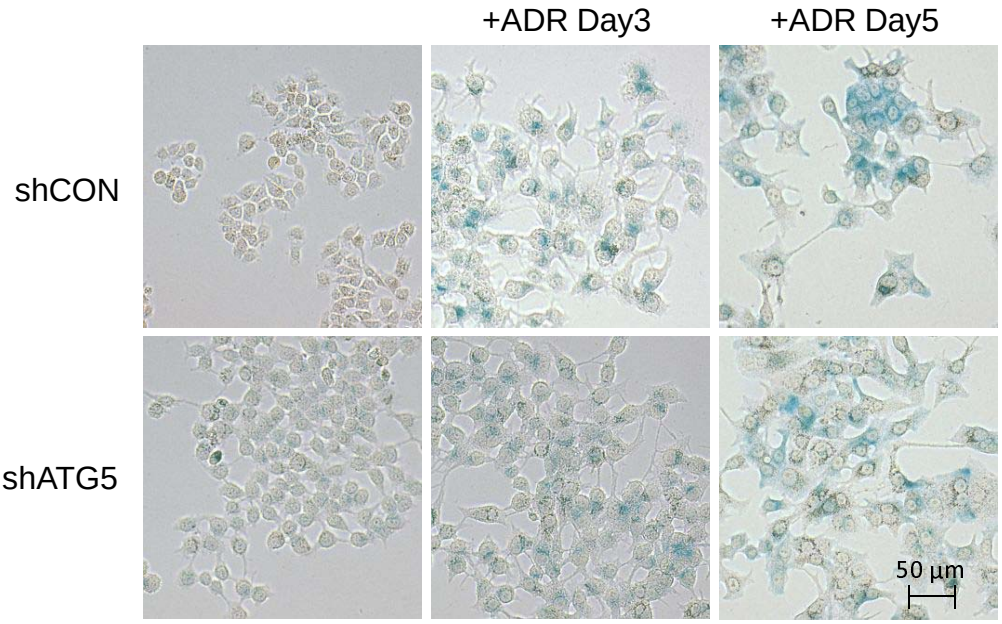

Lower Panel

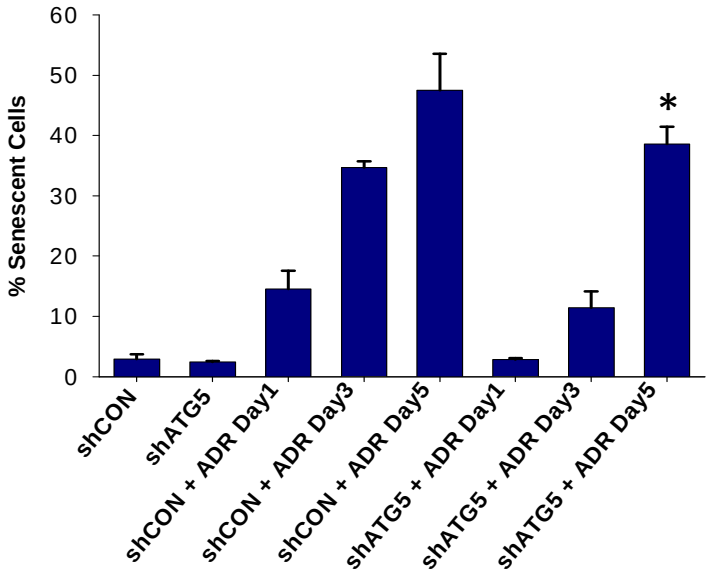

Figure 6

JPET Fast Forward. Published on August 27, 2012 as DOI: 10.1124/jpet.112.197590
This article has not been copyedited and formatted. The final version may differ from this version.

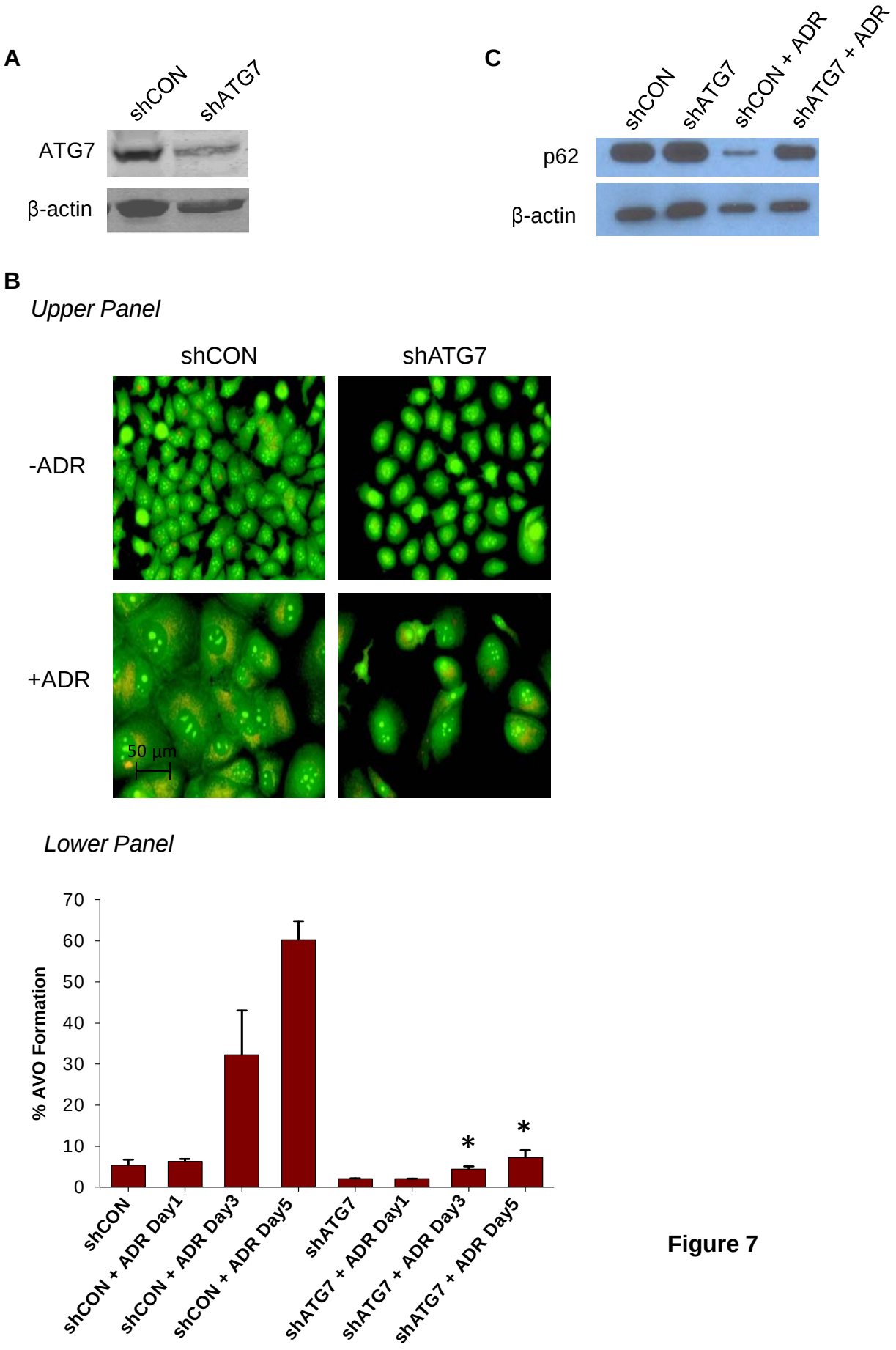

Figure 7

JPET Fast Forward. Published on August 27, 2012 as DOI: 10.1124/jpet.112.197590
This article has not been copyedited and formatted. The final version may differ from this version.

D

Upper Panel

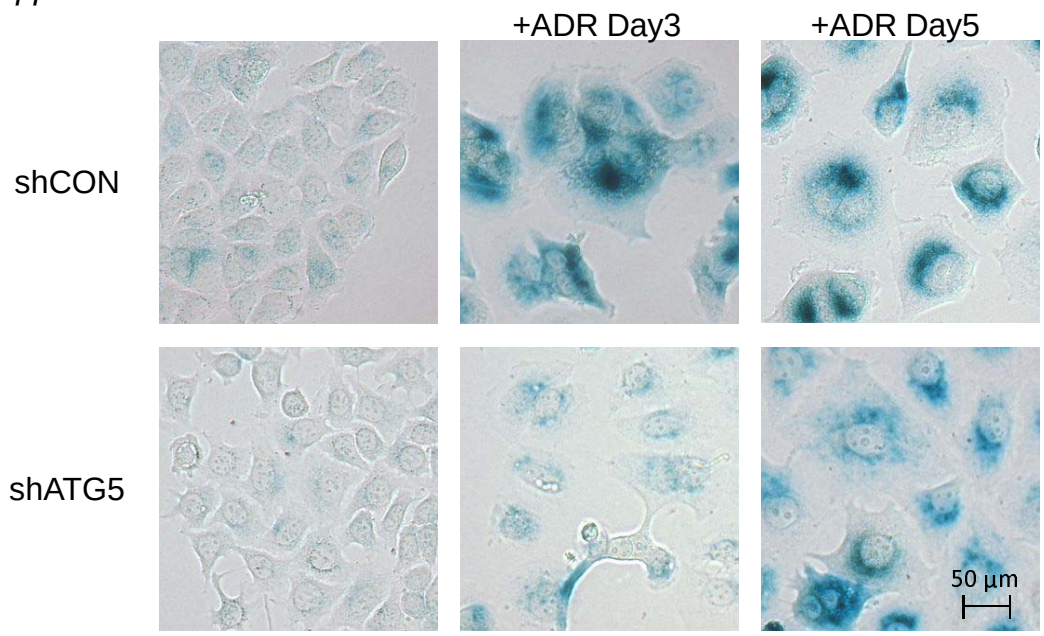

Lower Panel

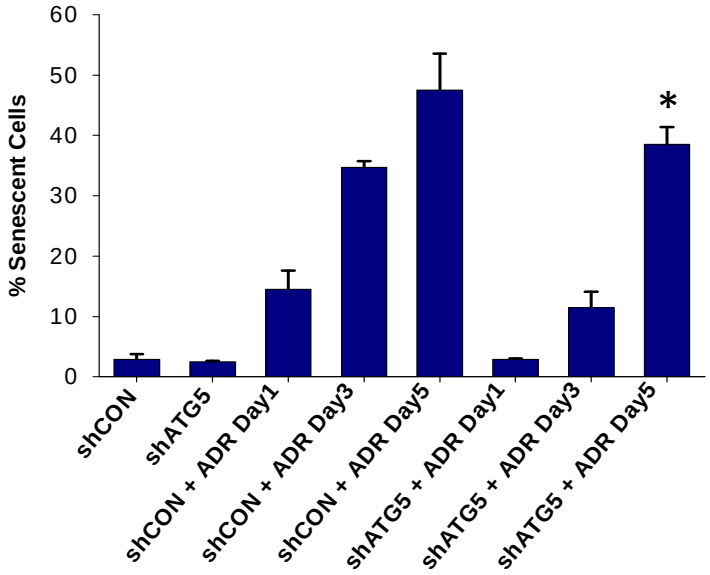

Figure 7

JPET Fast Forward. Published on August 27, 2012 as DOI: 10.1124/jpet.112.197590
This article has not been copyedited and formatted. The final version may differ from this version.

A

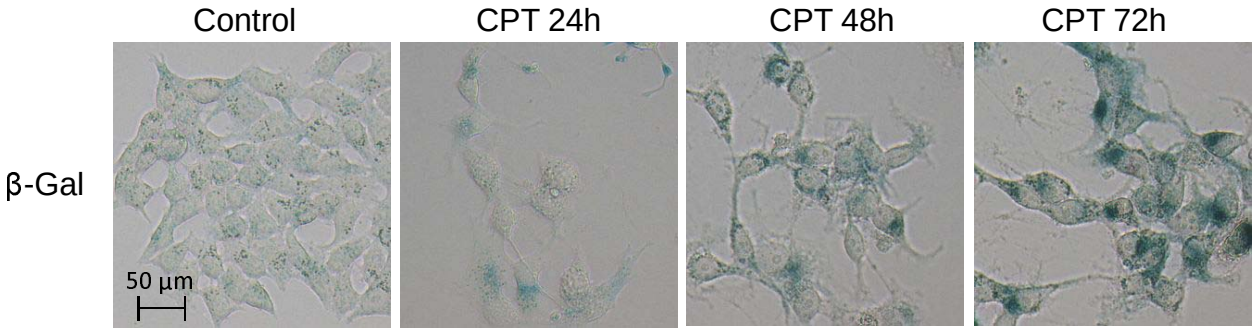

B

Left Panel

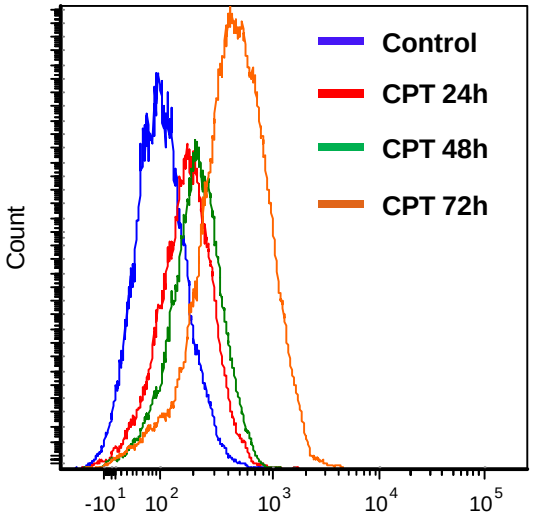

Right Panel

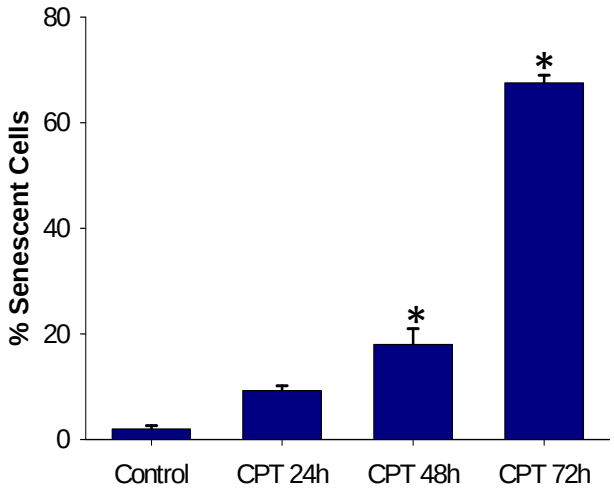

Figure 8

JPET Fast Forward. Published on August 27, 2012 as DOI: 10.1124/jpet.112.197590
This article has not been copyedited and formatted. The final version may differ from this version.

C

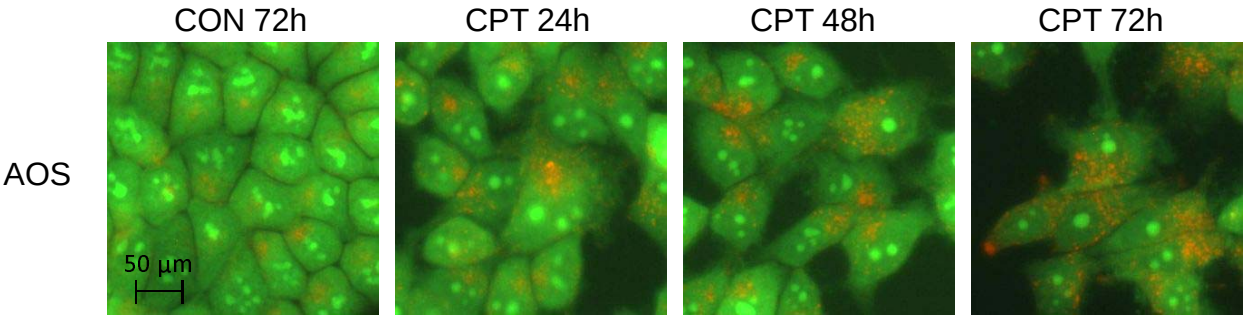

D

Left Panel

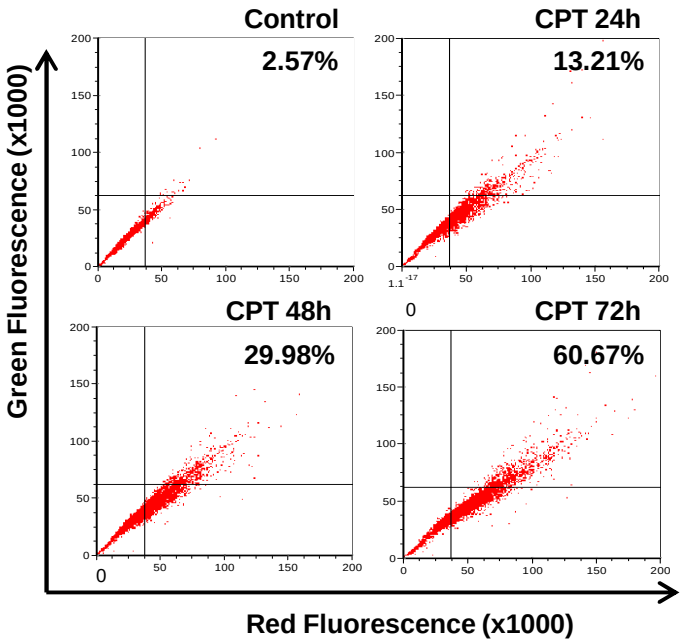

Right Panel

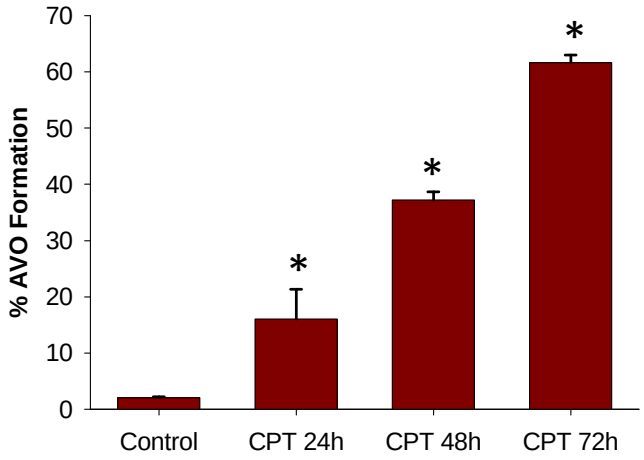

Figure 8

JPET Fast Forward. Published on August 27, 2012 as DOI: 10.1124/jpet.112.197590
This article has not been copyedited and formatted. The final version may differ from this version.

E

Upper Panel

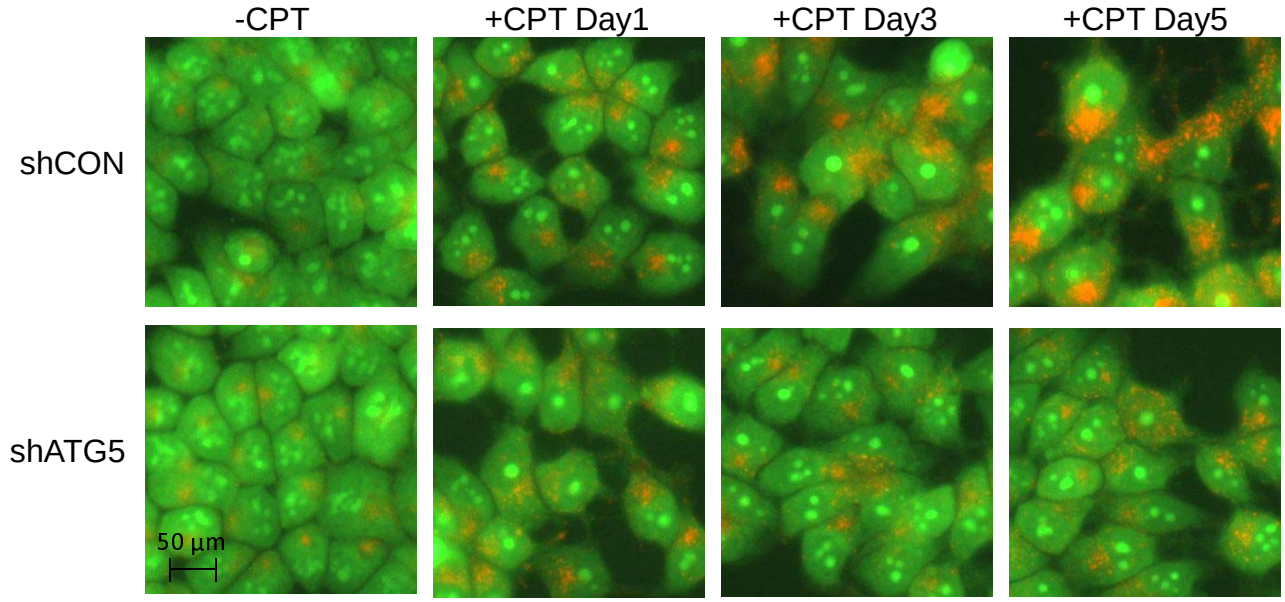

Lower Panel

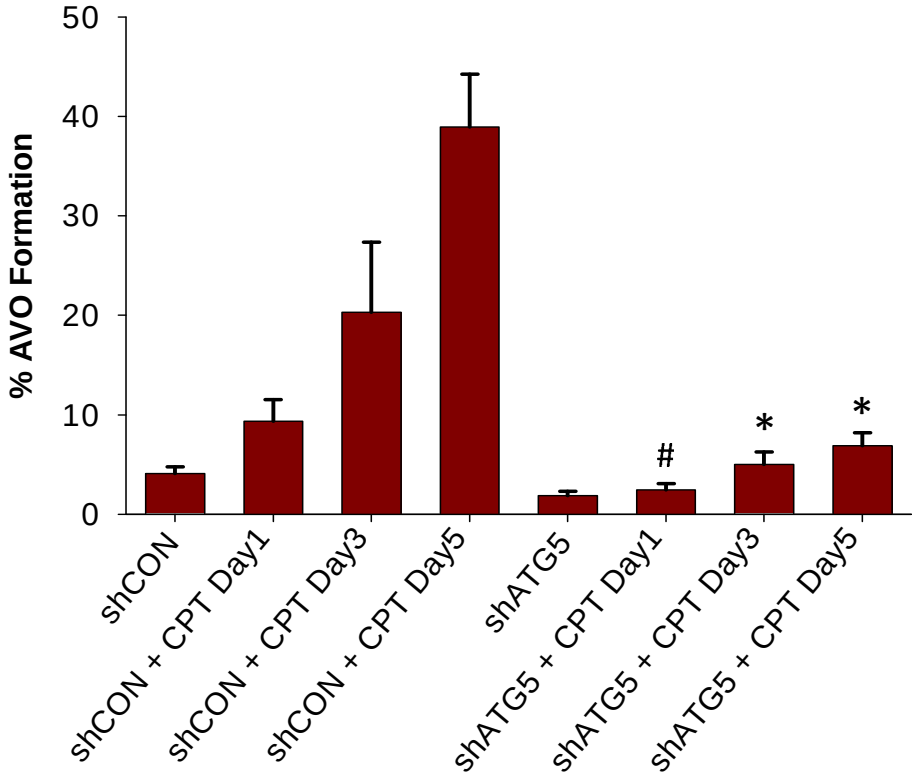

Figure 8

JPET Fast Forward. Published on August 27, 2012 as DOI: 10.1124/jpet.112.197590
This article has not been copyedited and formatted. The final version may differ from this version.

F

Upper Panel

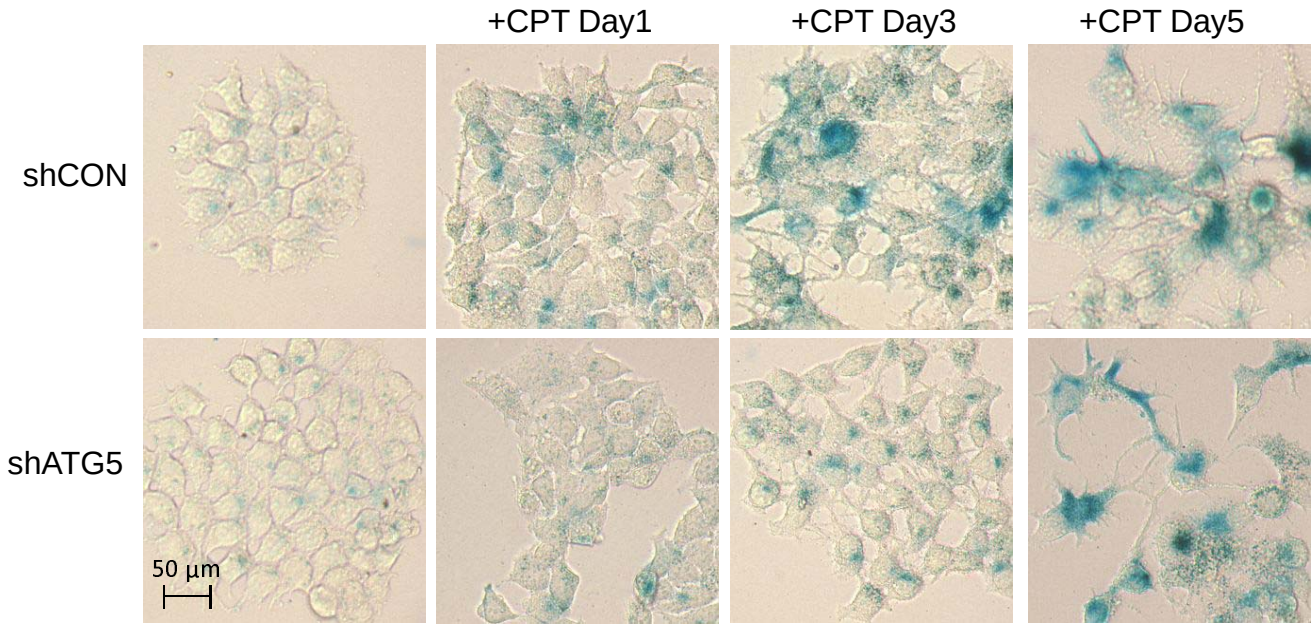

Lower Panel

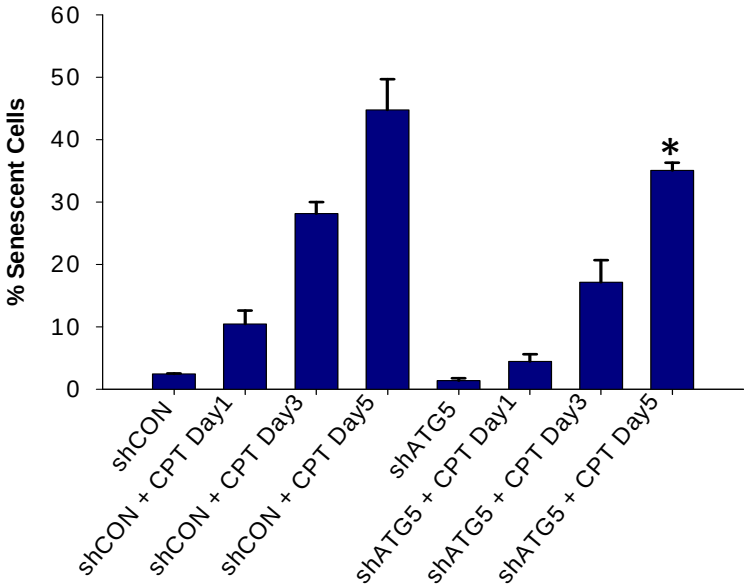

G

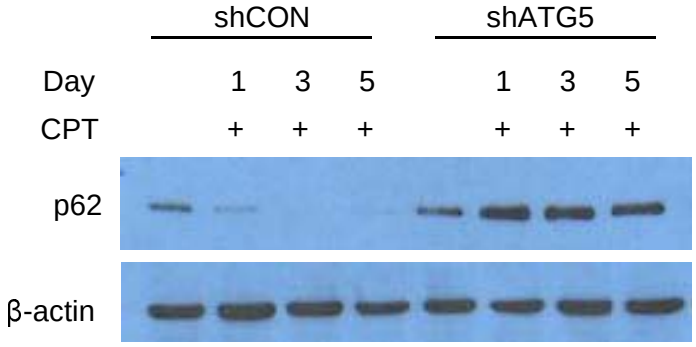

Figure 8